nature ecology & evolution

ARTICLES

https://doi.org/10.1038/s41559-020-1103-z

Chromosomal barcoding of *E. coli* populations reveals lineage diversity dynamics at high resolution

Weronika Jasinska[1,5], Michael Manhart[2,3,5], Jesse Lerner[1], Louis Gauthier[4], Adrian W. R. Serohijos[4] and Shimon Bershtein[1*]

Evolutionary dynamics in large asexual populations is strongly influenced by multiple competing beneficial lineages, most of which segregate at very low frequencies. However, technical barriers to tracking a large number of these rare lineages in bacterial populations have so far prevented a detailed elucidation of evolutionary dynamics. Here, we overcome this hurdle by developing a chromosomal-barcoding technique that allows simultaneous tracking of approximately 450,000 distinct lineages in *Escherichia coli*, which we use to test the effect of sub-inhibitory concentrations of common antibiotics on the evolutionary dynamics of low-frequency lineages. We find that populations lose lineage diversity at distinct rates that correspond to their antibiotic regimen. We also determine that some lineages have similar fates across independent experiments. By analysing the trajectory dynamics, we attribute the reproducible fates of these lineages to the presence of pre-existing beneficial mutations, and we demonstrate how the relative contribution of pre-existing and de novo mutations varies across drug regimens. Finally, we reproduce the observed lineage dynamics by simulations. Altogether, our results provide a valuable methodology for studying bacterial evolution as well as insights into evolution under sub-inhibitory antibiotic levels.

Sequencing advances have generated tremendous breakthroughs in the identification of beneficial mutations arising in laboratory evolution experiments, as well as mutations contributing to the emergence of anti-cancer or anti-bacterial drug resistance in clinical environments[1–4]. However, measuring the dynamics of evolutionary processes remains a major challenge, particularly in large asexual populations where many low-frequency, small-effect mutations are known to spread simultaneously[5–8]. A complete quantitative description of evolutionary dynamics therefore requires the tracking of a large number of individual lineages, most of which occur at extremely low frequencies (10^{-6} to 10^{-5}), in parallel and over multiple generations.

Whole-genome sequencing techniques currently fall short of fulfilling this requirement at typical read depths, because they are usually unable to detect mutations at frequencies below about 0.1%[9,10]. Various alternative solutions have been applied to reconstruct population dynamics from trajectories of individual lineages at much higher resolution than can be accessed by whole-genome sequencing[11–13]. One method that greatly increases the frequency resolution of individual lineages is based on tagging chromosomes of individual cells with a genetic 'barcode' that can be identified by deep sequencing[14]. Previous work implemented this approach in *Saccharomyces cerevisiae*, where chromosomal insertion of about 500,000 random barcodes using the Cre-*loxP* recombination system allowed a quantitative description of evolutionary dynamics of yeast populations (around 10^8 cells)[5,15,16]. In bacteria, however, technical barriers have limited the number of unique chromosomal barcodes to approximately 100–500[17–19]. Such low levels of barcode diversity preclude us from addressing important problems in bacterial evolution where high-resolution lineage tracking is essential. One such scenario is evolution in the presence of sub-inhibitory amounts of antibiotics, where the dynamics are driven by multiple mutations of low frequency and small fitness effects[20].

Here we present a method based on the Tn7 transposon to generate *E. coli* populations of $>10^7$ cells carrying 10^5–10^6 unique chromosomal barcodes. To demonstrate the utility of this technique, we evolved barcoded populations by serial passaging in the presence of sub-inhibitory concentrations of two common antibiotics, chloramphenicol and trimethoprim. Whereas previous studies on high-resolution microbial barcoding focused primarily on inferring the distribution of selection coefficients on new mutations[16], we pursued a complementary, ecology-inspired approach that focuses on tracking the diversity of lineages over time and across populations. This approach is amenable to a wider variety of conditions, such as time-varying environments and initial populations that already contain substantial genetic diversity. We found that different drug regimens elicited distinct and highly reproducible dynamics of lineage diversity. In particular, low amounts of trimethoprim unexpectedly slowed the rate of lineage diversity loss even beyond conditions of no antibiotic, hinting at the possibility that in this regime the antibiotic could be primarily functioning as a signalling molecule[21,22]. We also quantified the extent to which individual lineages had similar fates across replicate populations evolving in the same condition. Analysis of the dynamics of these lineages' frequency trajectories revealed the relative contributions of pre-existing mutations (standing genetic variations that arose prior to the experiment) versus de novo mutations (those acquired during the experiment). In general, stronger selection pressure generated faster loss of lineage diversity and more reproducible dynamics at the level of individual lineages owing to pre-existing beneficial mutations,

[1]Department of Life Sciences, Ben-Gurion University of the Negev, Beer-Sheva, Israel. [2]Department of Chemistry and Chemical Biology, Harvard University, Cambridge, MA, USA. [3]Institute of Integrative Biology, ETH Zurich, Zurich, Switzerland. [4]Department of Biochemistry, University of Montreal, Montreal, Quebec, Canada. [5]These authors contributed equally: Weronika Jasinska, Michael Manhart. *e-mail: shimonb@bgu.ac.il

whereas weaker selection produced slower diversity loss and less reproducible dynamics owing to a greater role of de novo mutations.

Results

Efficient chromosomal barcoding of *E. coli* cells. Several robust genome-editing methods available for *E. coli* have long made this organism a flagship of genetic manipulations[23]. A high-resolution chromosomal-labelling technique, however, has not been available, making it difficult to analyse the evolutionary dynamics of large bacterial populations segregating at low frequencies. To address this problem, we harnessed the well established site-specific recombination machinery of the Tn7 transposon[24,25]. We placed the *tnsABCD* genes, which encode the transposase biochemical machinery, under the control of an arabinose-inducible pBAD promoter in a temperature-sensitive 'helper' plasmid (Fig. 1a), while the Tn7 arms (Tn7L, Tn7R), which target the genetic cargo at a neutral *attnTn7* attachment site, are on a separate 'integration' plasmid (Fig. 1b). We placed the barcode cassette carrying a 15-nucleotide random sequence (the 'barcode') and the adjacent marker of selection between the Tn7 arms on the integration plasmid (Fig. 1b,c). To minimize the preparation of barcode libraries to two consecutive polymerase chain reaction (PCR) steps, we added sequences flanking the barcode cassette that are complementary to Illumina adapter primers (Fig. 1c). We used these sequences both to PCR-amplify barcodes directly on cell cultures as well as to anchor i5/i7 Illumina indices to the amplified barcodes (Methods). Using this Tn7 transposon system, we integrated barcodes into a fixed location on the *E. coli* chromosome in two steps (Fig. 1d). First, we transformed cells with the Tn7 helper plasmid and pre-conditioned them by inducing the transposase machinery. Second, we transformed the pre-conditioned cells with the barcoded integration plasmid. We simultaneously selected for chromosomal barcode integration and removal of the helper plasmid by plating on selective media and incubating the plates at 37 °C (Methods).

To assess the quality of the library preparation, we sequenced the barcode library at three points during the process: (1) the raw DNA library, as synthesized by the manufacturer and prior to incorporation of barcode cassettes into the integration plasmid (Methods); (2) the integration plasmid library, before incorporation into the chromosome; and (3) the library of barcodes successfully incorporated into the *E. coli* chromosomes. We identified about 1.3×10^6 unique barcodes in the raw library (Supplementary Table 1), with a fairly narrow distribution of frequencies: all barcodes but one had frequencies between 3×10^{-7} and 3×10^{-5} (Extended Data Fig. 1a). The nucleotide composition of these barcodes was also very close to random, as quantified by the entropy of nucleotides per position (Extended Data Fig. 1B). Incorporating the barcodes onto plasmids and then onto chromosomes reduced this diversity (about 8.4×10^5 unique barcodes on plasmids and about 4.6×10^5 on chromosomes; Supplementary Table 1). The process also introduced more redundancy into the distribution of frequencies, especially the chromosomal incorporation step, with some barcodes reaching frequencies of around 10^{-3} (Extended Data Fig. 1a). These increases in redundancy also led to a minor decrease in nucleotide entropy (Extended Data Fig. 1b). However, the presence of some barcodes with high initial frequencies did not appear to play a major part in the resulting lineage dynamics during evolution, as we show below.

We also compared the frequencies of individual barcodes between the different initial libraries, which showed a weak but significant correlation of frequencies between steps (Extended Data Fig. 1c,d); that is, barcodes that started at high frequencies tended to remain at high frequencies during the preparation process, but with fluctuations due to the incorporation procedure. To test the effect of noise from the PCR and sequencing processes, we also produced four independent sequencing replicates of the chromosomal library (Supplementary Table 1). The frequencies of individual barcodes across these replicates are strongly correlated (Supplementary Fig. 1), indicating that our sequencing and barcode identification methods are reproducible.

Laboratory evolution of the barcoded population. Bacteria are often exposed to antibiotic concentrations far below the minimal inhibitory concentration (MIC), both in natural environments and in patients receiving antimicrobial therapy[26,27]. Previous studies have shown that, compared to a lethal dosage, sub-MIC concentrations greatly expand the mutational space by allowing a large number of small-effect mutations to enter a population simultaneously[21]. The importance of low-frequency lineages in sub-MIC concentrations make these conditions a perfect setting in which to employ our barcoded population of *E. coli*. To this end, we chose two frequently used antibiotics with distinct modes of action: chloramphenicol (CMP), which inhibits protein synthesis via inactivation of peptidyl transferase activity of the bacterial ribosome[28]; and trimethoprim (TMP), which functions as a competitive inhibitor of the essential protein dihydrofolate reductase[29]. Previous work demonstrated that sub-inhibitory concentrations of antibiotics as low as 1% MIC can still select for resistant mutants over the wild type[30]. Therefore, we aimed for antibiotic concentrations around 1% MIC in our evolution experiments. Specifically, we identified concentrations that reduced the total number of cells by no more than 30% at the end of a single propagation cycle (about 10 h), compared to the untreated culture (Methods). These concentrations were 1 μg ml^{-1} CMP (6.25% MIC) and 0.1 μg ml^{-1} TMP (1% MIC) (Supplementary Fig. 2). To reduce the selection pressure even further below the minimal selective concentration, we also chose ultra-sub-MIC concentrations that were 10% of the aforementioned concentrations.

Altogether, we conducted laboratory evolution via serial passaging under five conditions: low CMP (6.25% MIC), ultralow CMP (0.625% MIC), low TMP (1% MIC), ultralow TMP (0.1% MIC) and a control without any drug (Extended Data Fig. 2a,b). We evolved 14 independent replicate populations under each of these five conditions (Extended Data Fig. 2c,d and Supplementary Table 2). We diluted batch cultures (500 μl each) grown in 96-well plates by 1:100 every 6 generations (that is, passaging twice daily; Extended Data Fig. 2e,f) with a bottleneck population size of about 3×10^7 cells (Extended Data Fig. 2c,d). To sustain the selection pressure during the evolutionary experiment (around 420 generations), we gradually increased the antibiotic concentrations for some of the conditions (Extended Data Fig. 2a,b and Supplementary Fig. 3; Methods). This helped to keep the number of cells at the end of each passage roughly constant along the entire evolutionary experiment for each population (Extended Data Fig. 2c,d). We randomly chose three replicate populations from each condition for all further analysis (sequencing and growth measurements), resulting in 15 total populations to consider.

We expected two major components of selection in the experiment: selection for traits that are beneficial to the specific type and concentration of antibiotic, and selection for traits that are beneficial under the general laboratory growth conditions (growth medium, aeration and so on). It is possible that there are tradeoffs between these two types of traits, that is, costs associated with the acquisition of drug resistance[31,32]. To assess the contributions of these factors, we measured two quantitative properties of each evolving population at several time points (Supplementary Table 3): the IC50 (antibiotic concentration inhibiting 50% of growth; Supplementary Fig. 4 and Methods), which provides an overall measure of the population's ability to grow in a specific antibiotic; and the growth rate in the absence of drug, which measures the adaptation of the populations to the general laboratory conditions and also measures possible costs of resistance. For populations evolving under the low CMP and low TMP conditions, the IC50 measurements revealed a moderate increase in antibiotic resistance over the evolution experiment

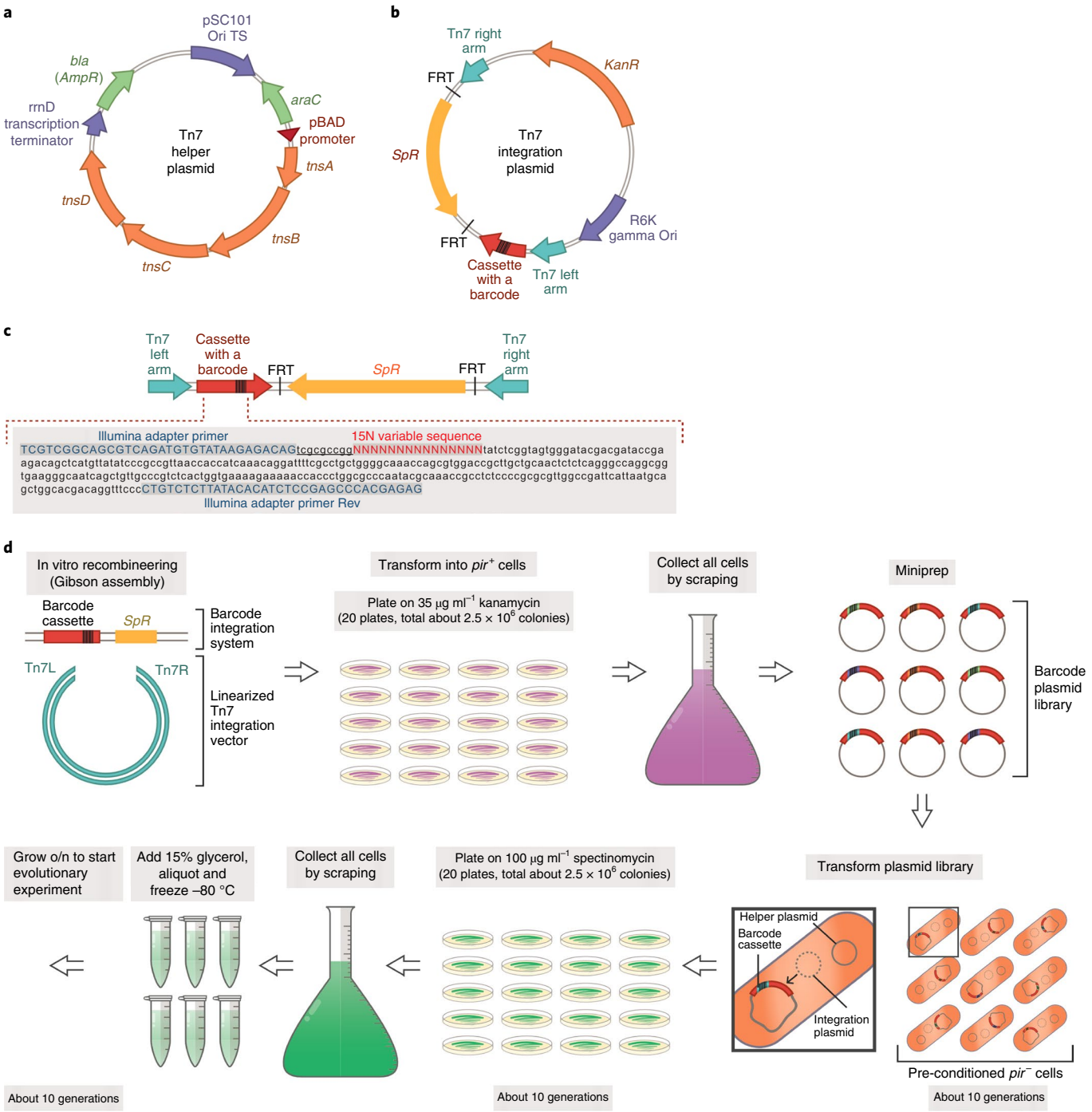

Fig. 1 | Barcoding *E. coli* cells with Tn7 transposon machinery. a, Map of the helper plasmid expressing the Tn7 transposon machinery (*tnsABCD*). **b**, Map of the integration plasmid carrying the barcode cassette and spectinomycin resistance-conferring gene (*SpR*) nested between the left and right Tn7 arms. **c**, Map of the segment undergoing chromosomal integration into the Tn7 attachment site (*attnTn7*). The inset shows the sequence of the barcode-carrying cassette. **d**, Steps for preparation of the barcoded plasmid and chromosomal libraries. See Methods for complete details. Recombineering is recombination-mediated genetic engineering, and Gibson assembly is a robust exonuclease-based method to assemble DNA fragments[55,56]. FRT, FLP Recognition Target sites, where FLP is a flippase that mediates excision of a DNA fragment flanked by FRT sites; this feature can be used to remove SpR gene from the chromosome[57]. *tnsA*, *tnsB*, *tnsC* and *tnsD* are genes encoding Tn7 transposase machinery and rrnD is a transcription terminator (detailed in ref. [25]). araC is an arabinose operon regulatory protein that regulates the expression from the arabinose promoter. o/n, overnight.

(Extended Data Fig. 3a,b). In contrast, both ultralow conditions, as well as the control without drug, produced no measurable improvement in IC50 measured at concentrations ≥1 μg ml^{-1} for CMP and ≥0.5 μg ml^{-1} for TMP (Extended Data Fig. 3a,b). Furthermore, the increases in drug resistance evolved under the low CMP and low TMP conditions were accompanied by a growth rate reduction in the absence of antibiotics (Extended Data Fig. 3c,d). In particular, the population that evolved to resist the highest levels of CMP (low CMP replicate 1, Extended Data Fig. 3a) showed the strongest growth rate reduction among the three replicate populations in the same condition (Extended Data Fig. 3c). However, we observed no growth rate cost in the populations evolved under ultralow CMP.

Instead, the growth rate trajectories for these populations were generally similar to those for the populations that evolved in the absence of antibiotics (Extended Data Fig. 3c). Surprisingly, in the populations evolved under ultralow TMP, the improvement in growth rate lagged behind that of the populations evolved under no antibiotics (Extended Data Fig. 3d), suggesting that the rate of adaptation to growth conditions at 0.1% MIC of TMP was diminished, despite the fact that we observed no improvement in TMP IC50 (Extended Data Fig. 3b).

Barcodes allow high-resolution monitoring of lineage trajectories. To elucidate the evolutionary dynamics of these populations at the level of individual lineages, we sequenced the barcodes of the same 15 populations at 16 time points (Supplementary Table 1). From the sequenced barcodes, we assembled frequency trajectories for all ~4.5×10^5 initial lineages over the course of the experiment (Fig. 2 and Extended Data Fig. 4). Plots of these trajectories immediately suggest several important qualitative insights. First, just one or two lineages dominated each population (>70%) by the end of the experiment (see also Supplementary Table 4). Second, some lineages rose to high frequency in multiple independent populations (lineage colours match across panels in Fig. 2 and Extended Data Fig. 4). Third, there is evidence of widespread clonal interference: some lineages that initially increased in frequency as a result of positive selection later decreased as a result of competition from higher-fitness lineages. Fourth, Fig. 2 suggests that the rate of lineage diversity loss was reproducible between replicate populations under the same conditions, while systematically distinct across different conditions. This implies that condition-specific selection, rather than selection for general laboratory conditions or neutral dynamics, dominated the lineage dynamics at the whole-population level. Indeed, although genetic drift causes the loss of many individual low-frequency lineages, approximately $2N$ generations (where N is the effective population size) are required for a single lineage to fix by genetic drift alone[33]. Since the effective population size in our experiments was of the order of 10^7 (Extended Data Fig. 2c,d), neutral dynamics cannot be responsible for the overall loss of lineage diversity we observe, which includes near-fixation in several populations.

Quantifying lineage diversity dynamics across conditions. To quantify the dynamics of lineage diversity, we adopted a measure of diversity widely used in ecology, the diversity index[34,35]:

$$ {}^{q}D = \left(\sum_{\text{lineage } k} x_k^q \right)^{1/(1-q)} \qquad (1) $$

where x_k is the frequency of the kth barcoded lineage and q is the 'order' of the diversity index, which determines the sensitivity of diversity to abundant versus rare barcodes (Methods). In general, we can interpret the diversity index as the effective number of lineages present in the population. When $q=0$, the diversity index simply counts the number of unique barcoded lineages, irrespective of their frequencies. This case is equivalent to measuring diversity as 'species richness' in ecological contexts[34]. When $q=1$, the diversity index weights all barcoded lineages by their frequencies, which is sometimes known as the Shannon diversity because it is equivalent to the exponential of the Shannon entropy of the frequencies. In the limit of $q\to\infty$, the diversity index equals the reciprocal of the maximum lineage frequency, meaning that it depends only on the most abundant lineage and no others. Thus, by comparing the lineage diversity index across different q values, we can estimate the relative contributions of rare and abundant lineages to that diversity. We note that if all lineages have equal frequencies, then the diversity index equals the actual number of lineages for any value of q. We emphasize that 'diversity' here refers to the diversity of lineages descending from the initial population, meaning that it must decrease monotonically over time, unlike the genetic diversity of the population, which can increase owing to new mutations.

We first tested the diversity index on the initial barcode libraries. For each of the initial barcode libraries (raw DNA library, plasmid library and chromosomal library; Extended Data Fig. 1), we calculated the diversity index in equation (1) for $q=0$, $q=1$ and $q=\infty$ (Supplementary Fig. 5a). As expected, we see that the diversity decreased at each step of the library preparation (except for ${}^{\infty}D$ in going from the raw library to the plasmid library, which suppressed the frequency of the most-frequent barcode; see Extended Data Fig. 1a). We also see that the diversity index decreases as the order q increases, since increasing the weight of higher-frequency lineages reduces their effective number. Indeed, the total number of unique chromosomal barcodes is ${}^{0}D \approx 4.5\times10^5$ (Supplementary Fig. 5a, left panel), but the effective number of lineages, using $q=1$ to weight them by their unequal frequencies (Extended Data Fig. 1a), is approximately ten-fold lower, ${}^{1}D \approx 4.6\times10^4$ (Supplementary Fig. 5a, centre panel). To test the robustness of the diversity index to noise in the PCR and sequencing process, we also calculated the diversities of the four replicate samples of the initial chromosomal library (Supplementary Fig. 5a). Although there is noise at the level of individual low-frequency barcodes across these replicates (Supplementary Fig. 1), the diversity indices are highly reproducible, with all replicates falling within 10% of each other for all q values (within 2% for $q=1$). Furthermore, while pooling these replicate samples increases the total number of unique barcodes ${}^{0}D$ by 70–80% (Supplementary Fig. 5a, left panel), it only increases the $q=1$ diversity by 5% to 6% (Supplementary Fig. 5a, centre panel). Therefore, while sampling noise in the sequencing process can have an important effect on estimates of the absolute number of barcodes, the effective number is relatively robust at the sampling and sequencing depths we are using.

We now turn to assessing the diversity of the populations in the evolution experiment. Figure 3a shows the effective number of lineages for each population over the time of the experiment, using three different values of q. Low CMP produced the fastest collapse of lineage diversity, extinguishing over 90% of unique barcodes in less than 50 generations. This behaviour was displayed at all q values, indicating that rare and frequent barcodes contributed equally to these dynamics. In contrast, populations under low TMP conditions lost ${}^{0}D$ diversity more rapidly compared to the ultralow CMP and no drug conditions, but it lost ${}^{1}D$ and ${}^{\infty}D$ diversities at approximately the same rate; this indicates that the dynamics of abundant lineages were similar for these three conditions, but that low-frequency lineages disappeared more quickly under low TMP. More surprising was the fact that populations under ultralow TMP lost diversity even more slowly than did populations under no drug. Indeed, the diversity of populations under ultralow TMP maintained 40% to 50% of the initial effective diversity ($q=1$) up to approximately generation 120, whereas populations with no drug had only about 1% of their initial diversity by that time point. This difference in the rates of lineage diversity deterioration between the ultralow TMP and no drug conditions is consistent with our measurements of growth rate reduction in the absence of drug, wherein the rate of adaptation under ultralow TMP lagged behind that of no drug populations (Extended Data Fig. 3d). Interestingly, ${}^{0}D$ diversity under ultralow TMP was similar to the other populations by about generation 250, but its diversity at larger q remained higher until the very end of the experiment. Towards the end of the experiment, we saw that the effective diversity of all populations is 1–5 lineages (${}^{1}D$), consistent with the observations from Fig. 2. However, we note that despite the drop in lineage diversity, there was still an ample number of surviving barcode lineages: each population retained a few thousand barcodes by the end of the experiment, as seen in ${}^{0}D$ (Fig. 3a).

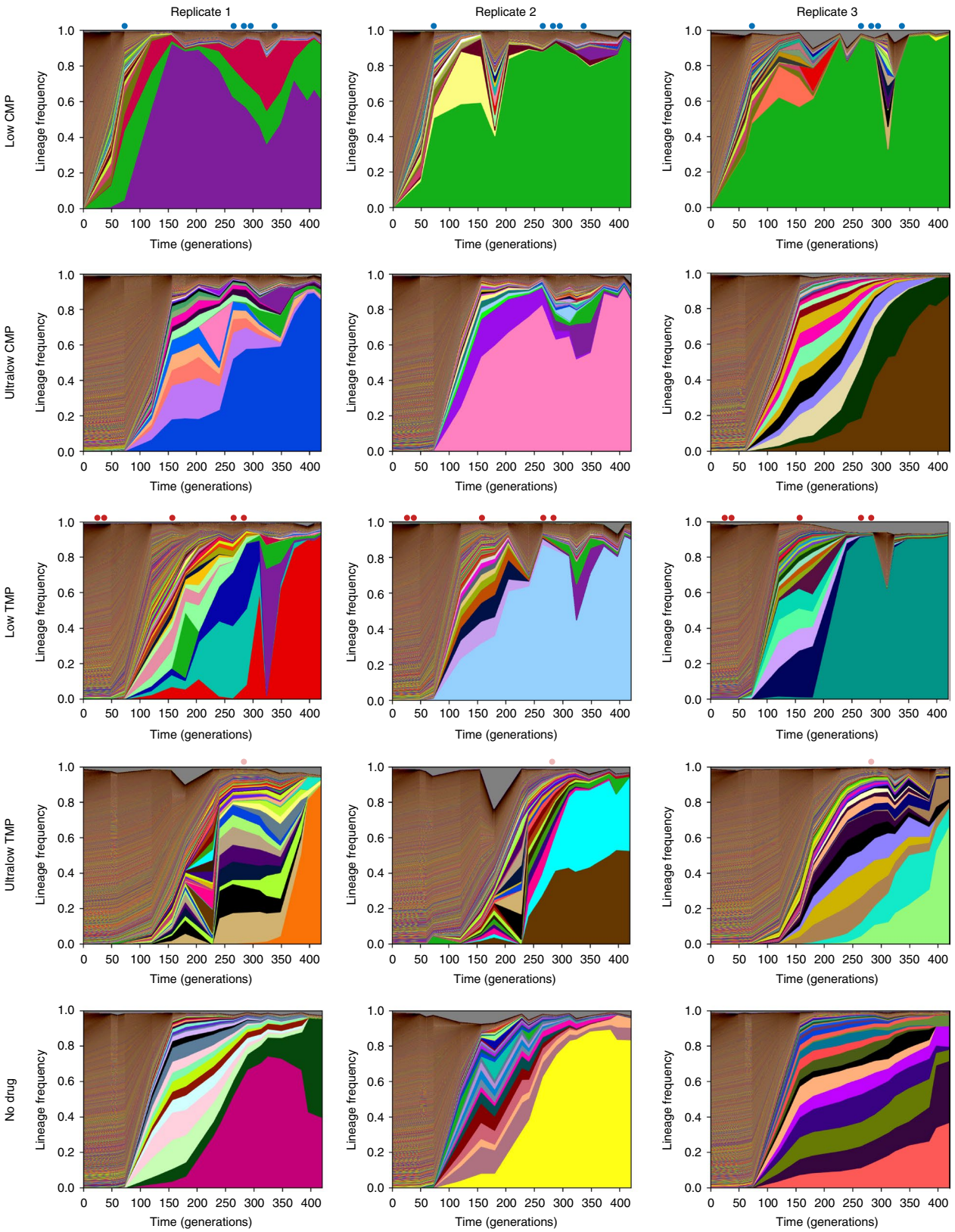

Fig. 2 | Dynamics of barcoded lineage frequencies over evolution experiment. Each row corresponds to a different antibiotic regimen, while each column corresponds to a different replicate. Individual panels show the frequency trajectories for all barcoded lineages in single populations over time of the experiment. Each coloured band corresponds to a unique lineage, with its vertical width indicating its frequency at a particular time point. For the top 20 lineages in each population (ranked by mean frequency over time), we assign a unique colour to each lineage that is consistent across panels, that is, the same colour represents the same barcode across panels (Supplementary Table 4). We use random colours for all lower-frequency lineages. The grey band at the top represents the frequency of reads without identified barcodes. Dots above each plot mark times at which the drug concentration for that population changed (Extended Data Fig. 2a,b).

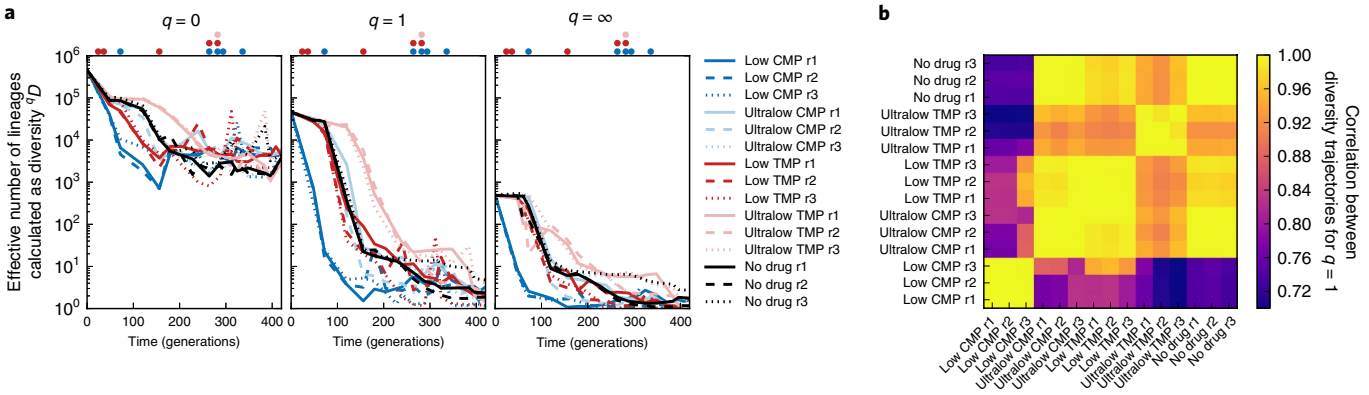

Fig. 3 | Dynamics of lineage diversity over time. a, For each population and at each time point, we measured the effective number of barcoded lineages using the diversity index ${}^{q}D$ (equation (1); see also Methods) for three different values of q, which controls the weight of low- versus high-frequency lineages: ${}^{0}D$ (number of unique barcodes, left), ${}^{1}D$ (Shannon diversity, centre), and ${}^{\infty}D$ (reciprocal of the maximum lineage frequency, right). Dots above each plot mark times at which drug concentrations changed (Extended Data Fig. 2a,b); their colours indicate the drug environment according to the key. **b**, Pearson correlation coefficient between diversity trajectories (for ${}^{1}D$) from all pairs of populations. r1, replicate 1; r2, replicate 2; r3, replicate 3.

Reproducibility of individual lineage dynamics. Not only did different antibiotic regimens produce distinct patterns of lineage diversity loss, but we also observed that these patterns are consistent across replicate populations. In Fig. 3b we show the Pearson correlation coefficients between the ${}^{1}D$ diversity trajectories from all pairs of populations. Although all trajectories are somewhat correlated because they must monotonically decrease, we saw stronger similarity among trajectories from the same conditions. To further dissect whether individual lineages have similar fates across populations, we must quantify the similarity between lineage frequencies in different populations.

To compare the lineage composition of two or more populations at a single time point, we used a definition of diversity dissimilarity from ecology (Methods). Suppose we have M populations whose lineage compositions we want to compare. We first calculate the diversity index (equation (1)) for all M populations pooled together, ${}^{q}D_{\text{pooled}}$. We then calculate the diversity index for each population alone and determine the mean across all populations, ${}^{q}D_{\text{mean}}$. The ratio of these two quantities, shifted and rescaled, measures the dissimilarity among lineage compositions, calculated as[34,35]:

$$\frac{{}^{q}D_{\text{pooled}}/\,{}^{q}D_{\text{mean}} - 1}{M - 1} \qquad (2)$$

If the lineage compositions of all populations are identical, then the pooled population has diversity equal to the mean diversity, and so the dissimilarity equals zero. In contrast, if the lineage compositions of M populations have no overlap, then the pooled population has diversity M times greater than that of the mean single population, and so the dissimilarity index equals 1. As with the diversity index, the parameter q allows us to vary the importance of low- and high-frequency lineages in the overall lineage dissimilarity. For $q=0$, lineage dissimilarity measures how many lineages multiple populations have in common, regardless of their frequencies, while for $q\to\infty$, it compares only the highest-frequency lineages (Methods).

We first tested the measure of lineage dissimilarity by calculating it between all pairs of initial barcode libraries (Supplementary Fig. 5b). We see very low dissimilarity among the sequencing replicates of the chromosomal library; for example, the $q=1$ dissimilarity among the chromosomal replicates is about 3% (Supplementary Fig. 5b, centre panel). As with the diversity indices themselves, we see little effect of pooling samples to increase read depth, indicating that our read depth is sufficient. This analysis furthermore confirms that the largest change in barcode frequencies occurs during incorporation of the plasmid library onto the chromosomes, as the raw library and plasmid library are more similar to each other than to the chromosomal libraries (Supplementary Fig. 5b; see Extended Data Fig. 1c,d).

We then calculated the dissimilarity across all evolved populations at each time point. In Fig. 4a (left panel), we show the $q=1$ dissimilarity between all pairs of populations at generation 120. At the beginning of the experiment, the populations were identical and so the dissimilarity between all pairs of populations was zero. By generation 120, we see that many pairs of populations from different conditions have already diverged (dissimilarity close to the maximum value of 1), while pairs of populations from the same conditions remained more similar (except for low TMP). Furthermore, we see some similarity even between conditions: populations under the weakest antibiotic pressures (ultralow CMP, ultralow TMP and no drug) all maintained similarity between conditions comparable to their similarity between replicates. However, by the end of the experiment at generation 420 (Fig. 4a, right panel), most of the similarity between populations disappeared. The main exception was for low CMP, where the three replicate populations maintained strong similarity. There was also a small amount of residual similarity among the populations for low CMP, ultralow CMP (two out of three replicates) and low TMP (two out of three replicates). In contrast, replicate populations under the ultralow TMP and no drug conditions showed no similarity among each other by the end of the experiment. There was also strong similarity between replicate 3 in ultralow CMP and replicate 2 of ultralow TMP.

We can further quantify the reproducibility of lineage dynamics by calculating diversity dissimilarity among all replicate populations under each condition over time (Fig. 4b and Supplementary Fig. 6). For $q=0$, we see that the dynamics of within-condition dissimilarity were similar to the dynamics of the diversity indices themselves in Fig. 3a. That is, populations under low CMP diverged from each other most rapidly, followed by those under low TMP, then by those under ultralow CMP and no drug concurrently, and finally with those under ultralow TMP diverging last. Interestingly, all conditions settled at an intermediate amount of around 0.8 dissimilarity for $q=0$ by the end of the experiment; this value corresponds to having about 20% of their lineages in common (Methods). The $q=1$ lineage dissimilarity, which accounts for heterogeneity in lineage frequencies, shows some differences with the $q=0$ case, which simply counts barcodes. With $q=1$, low CMP populations actually diverged more slowly from each other than did populations in the other conditions. Moreover, the low CMP populations

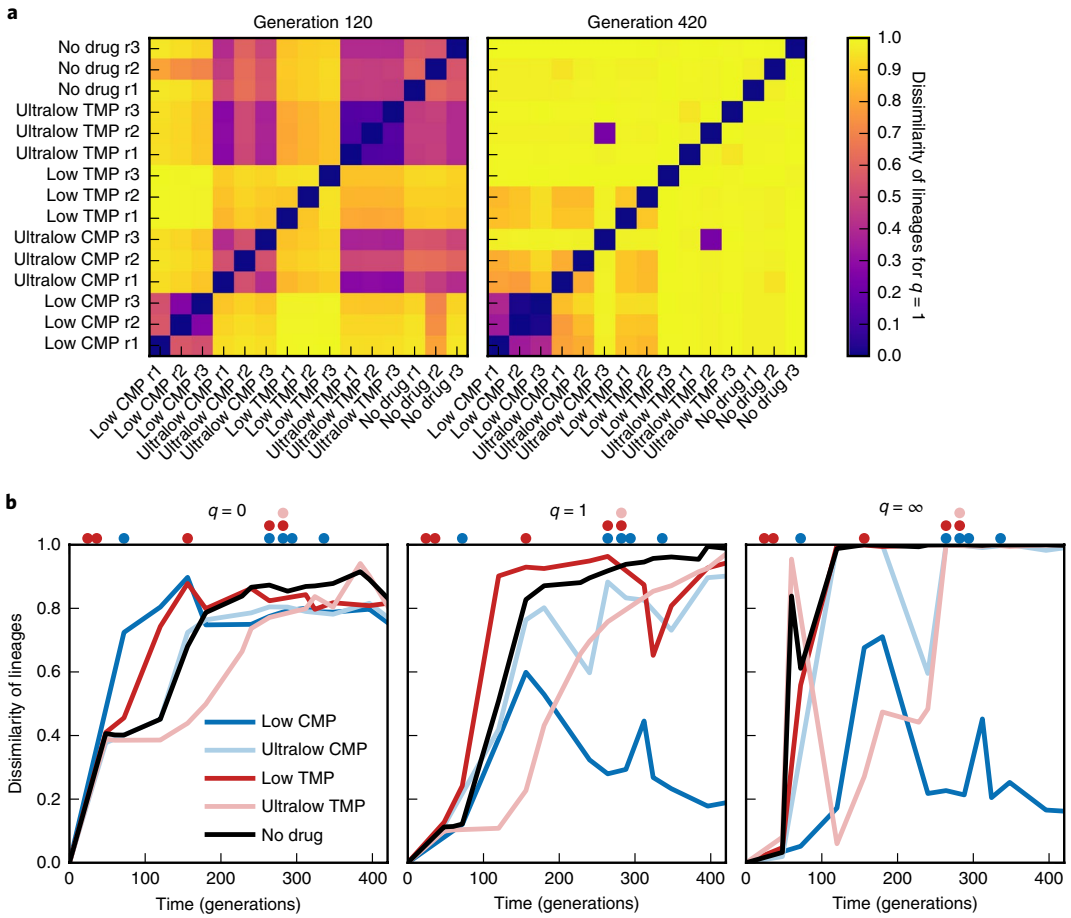

Fig. 4 | Dynamics of lineage dissimilarity among populations over time. a, Dissimilarity of lineages for $q=1$ (equation (2); see also Methods) between all pairs of populations at generation 120 (left) and the final time point at generation 420 (right). **b**, Dissimilarity of lineages among all replicate populations in each drug condition, using $q=0$ (left), $q=1$ (centre) and $q=\infty$ (right). Dots above each plot mark times at which the drug concentrations changed (Extended Data Fig. 2a,b); their colours indicate the drug environment according to the key.

actually reached some maximum level of $q=1$ dissimilarity around generation 150, and then began converging toward more similar lineage compositions. At the other extreme, ultralow TMP and no drug populations reached maximum dissimilarity by the end of the experiment, while low TMP and ultralow CMP populations had an intermediate value of dissimilarity. The dissimilarity index with $q=\infty$ shows a similar pattern of rise and fall for low CMP populations; since this case depends only on the most frequent lineage, it implies that the high level of similarity between low CMP populations by the end of the experiment was due to their sharing of the same dominant lineage.

Altogether, this analysis shows that lineage dynamics under identical conditions are highly reproducible, even at the level of individual lineages. Specifically, it suggests that some lineages repeatedly rose to high frequency over multiple experiments. To demonstrate this more explicitly, in Fig. 5a,b we compare the frequencies of all barcoded lineages at the end of the experiment for three replicate populations under low CMP conditions. Furthermore, in Fig. 5c we show the overlap of the top ten barcodes (ranked by mean frequency over time) between all three replicate populations under low CMP conditions: four of the top ten in each population are shared among all replicates, with three more barcodes shared between two replicates (see also Supplementary Table 4). Indeed, the most frequent lineage in replicates 2 and 3 is the same lineage (green trajectories in Fig. 2); this lineage is also the second-most frequent lineage in replicate 1. In contrast, Fig. 5d–f shows the same plots for the no drug populations, which have little similarity among their most frequent lineages. In particular, the only overlap between their top ten barcodes is one barcode shared between replicates 2 and 3 (Fig. 5f and Supplementary Table 4). In Supplementary Figs. 7 and 8 we show direct comparisons of lineage frequencies between all pairs of populations.

One possible explanation for the repeated dominance of certain lineages is that those lineages may have started at unusually high frequencies (Extended Data Fig. 1a). However, several lines of evidence refute this possibility. In Supplementary Fig. 9 we compare the initial and final frequencies for all lineages in each population. In general, the final frequencies are poorly correlated with the initial frequencies; in particular, the initial frequencies of the lineages that dominate at the end of the experiment are often below or very near the average initial frequency (grey vertical bars in Supplementary Fig. 9). We also calculate the lineage dissimilarity of each population at each time point compared to the initial population (Supplementary Fig. 10); this also shows that the evolved populations are almost maximally dissimilar from the initial populations, indicating that the initial frequencies of lineages are largely independent of their final values.

Individual lineage trajectories reveal the relative contributions of pre-existing and de novo mutations. To further probe the striking amount of similarity among some populations at the level of individual lineages, we first note that many lineages within populations

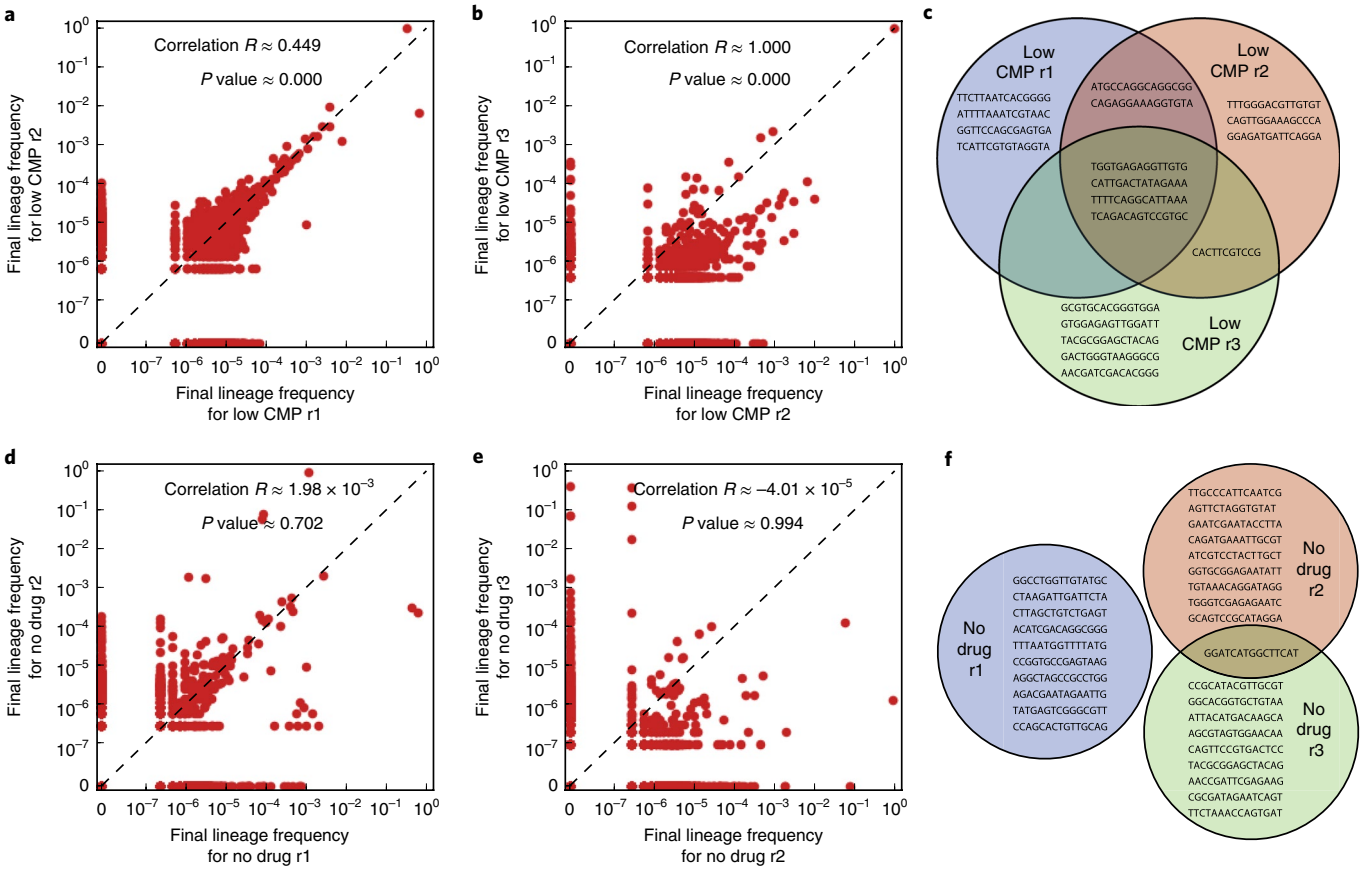

Fig. 5 | Reproducibility of individual lineage dynamics. a,**b**, Comparison of final frequencies of all barcoded lineages under low CMP conditions between replicate populations 1 and 2 (**a**) and between replicate populations 2 and 3 (**b**). The dashed black line marks the line of identity; each panel also shows the Pearson correlation coefficient *R* and estimated *P* value for the frequencies (*P* values are numerically indistinguishable from zero). **c**, Venn diagram of the top ten barcodes (ranked by mean frequency over time) in each replicate population from low CMP. **d**–**f**, Same as **a**–**c** but for three replicate populations without drug.

appear to follow similar trajectories (Extended Data Fig. 4). We therefore performed hierarchical clustering of a subset of high-frequency lineage trajectories in each population, based on the correlation coefficients between trajectories (Supplementary Figs. 11 and 12; see also Methods). The trajectories indeed formed well defined clusters with distinct dynamics (Supplementary Fig. 13); in particular, similar clusters appeared in replicate populations from the same condition, while clusters in populations from different conditions appeared to be more dissimilar. A few clustered trajectories also shared barcodes with very similar sequences, suggesting these lineages are actually the same (that is, the apparently distinct barcodes arose from sequencing errors; Supplementary Fig. 14); however, the vast majority of clustered trajectories involved unrelated barcode sequences, suggesting they are truly distinct lineages with highly correlated dynamics.

The clustering analysis revealed two key types of adaptive trajectories. Trajectories of the first type increased immediately at the beginning of the experiment, before later getting outcompeted by other lineages (Fig. 6a, left panel). The initial increase suggests that these lineages carried pre-existing beneficial mutations at the beginning of the experiment; these mutations were presumably acquired during the approximately 30 generations of growth that occurred during preparation of the barcode library (Fig. 1d). Trajectories of the second type were initially flat and started to increase only later in the experiment (Fig. 6a, right panel); these lineages presumably acquired beneficial mutations de novo during the experiment. To test these interpretations, we identified trajectories of both types in each population (Supplementary Fig. 13) and compared the lineages in each type across populations; lineages with pre-existing mutations should show the same behaviour across multiple populations, while lineages with de novo mutations should not. Indeed, we see substantial overlap in lineages with putative pre-existing mutations across populations (Fig. 6b, left panel), while almost no overlap can be observed in lineages with putative de novo mutations (Fig. 6b, right panel). We also compared the initial frequencies of trajectories in both types of clusters; a set of lineages carrying pre-existing mutations with similar selection coefficients (and which therefore cluster together) should have more similar initial frequencies owing to their similar growth dynamics during library preparation, whereas lineages that acquire only de novo mutations later should have unrelated, more variable initial frequencies. We find that trajectories with putative pre-existing mutations do in fact have somewhat less variable initial frequencies on average (Supplementary Fig. 15; Welch's *t*-test, *P* value ≈ 0.03).

To assess the overall contributions of pre-existing and de novo beneficial mutations to the evolutionary dynamics, we summed all trajectories of each type in each population (Fig. 6c). For low CMP, the lineages with pre-existing beneficial mutations dominated from the beginning of the experiment (Fig. 6c, left panel); in fact, we observed no trajectories with the signature of de novo mutations in this condition (Supplementary Fig. 13). This does not mean that no de novo mutations occurred in this condition, but rather that they apparently occurred on the background of lineages with pre-existing beneficial mutations. For example, the dominant purple lineage

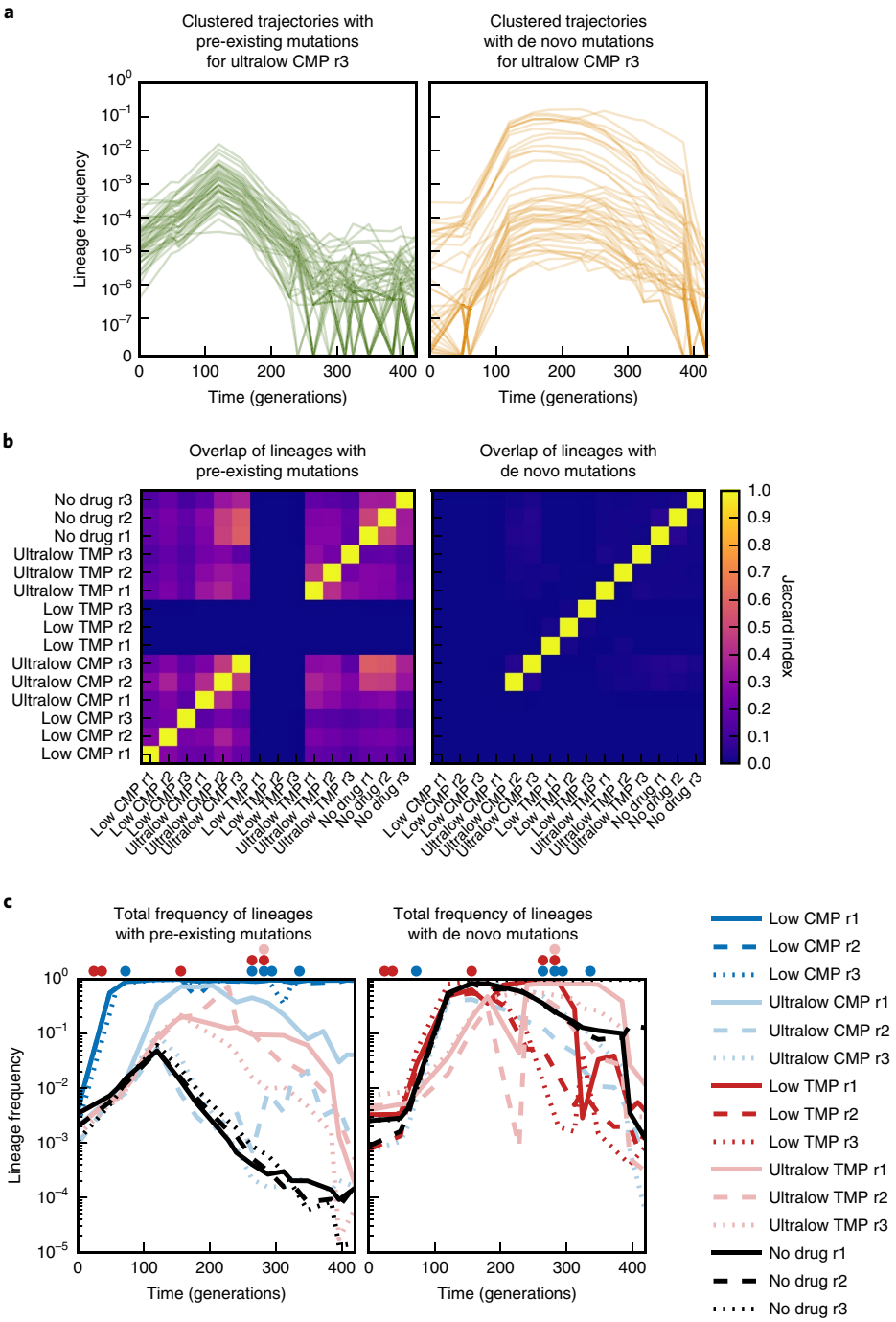

Fig. 6 | Distinct patterns of trajectories from pre-existing and de novo beneficial mutations. a, Examples of clustered lineage trajectories suggesting the presence of pre-existing beneficial mutations (left) and de novo beneficial mutations (right) from ultralow CMP replicate 3. Trajectories are partially transparent to show overlap. **b**, For each pair of populations, we calculated the relative overlap of lineages in trajectory clusters with apparent pre-existing beneficial mutations (left) and in clusters with apparent de novo beneficial mutations (right) (see Supplementary Fig. 13 for classification of trajectory clusters). We measured overlap using the Jaccard index, that is, the ratio of the number of lineages in the intersection to the number in the union. All entries are zero for pre-existing mutations under low TMP and for de novo mutations under low CMP because we identify no clusters of these types in those populations (Supplementary Fig. 13). **c**, Total frequency trajectories of all lineages with apparent pre-existing mutations (left) and with apparent de novo mutations (right) in each population. Dots above each plot mark times at which the drug concentrations changed (Extended Data Fig. 2a, b); their colours indicate the drug environment according to the key.

in replicate 1 (Fig. 2) appears to have acquired at least a second strongly beneficial mutation around generation 324. The existence of strongly beneficial pre-existing mutations under low CMP conditions explains why these populations demonstrated such strong convergence in lineage composition (Figs. 4 and 5a–c). In contrast, most other populations show a balance between lineages with pre-existing mutations and lineages with de novo mutations, with pre-existing mutations driving the initial dynamics and de novo mutations dominating later. For example, the populations evolving under the no drug conditions also have lineages with apparent

pre-existing beneficial mutations (Fig. 6c, left panel), but they rapidly lost frequency after about generation 120, when the lineages with de novo mutations took over (Fig. 6c, right panel). This is also consistent with the low level of convergence we see in these populations (Figs. 4 and 5d–f). Finally, we note that the populations under the ultralow TMP and no drug conditions appear to have similar selection on their trajectories with pre-existing mutations (Fig. 6c, left panel), even though populations under the ultralow TMP condition lost their diversity much more slowly than did the populations under the no drug condition (Fig. 3a). The difference arose for the de novo mutations, which appeared to be under much weaker selection under the ultralow TMP condition than under the no drug condition (Fig. 6c, right panel).

Lineage dynamics under constant drug conditions. In the above-mentioned evolution experiment, we increased the concentrations of drugs in some conditions to maintain approximately constant selection pressure as the populations adapted (Extended Data Fig. 2). To verify the robustness of those results, we repeated the evolution experiments in conditions with constant rather than changing drug concentrations, and with consistent bottlenecking every 12 h (Methods). We also sequenced the barcodes at several earlier time points to better capture the initial dynamics (Extended Data Fig. 5 and Supplementary Fig. 16).

Evolution with constant concentrations recapitulated all the major conclusions of the original experiment in increasing concentrations (Extended Data Figs. 6–8 and Supplementary Figs. 17 and 18). In particular, constant low CMP again produced the fastest loss of lineage diversity (Extended Data Fig. 6a; see Fig. 3a). The lineage dissimilarity of these populations also diverged more quickly with $q=0$ but more slowly with $q=1$ compared to the other populations (Extended Data Fig. 7b; see Fig. 4b), indicating the dominance of pre-existing beneficial mutations, which were again identified by clustering the lineage trajectories (Extended Data Fig. 8b; see Fig. 6c). We also recovered the effect of TMP on slowing diversity loss compared to no drug; however, in the second experiment this occurred for the low TMP condition rather than for the ultralow TMP condition (Extended Data Fig. 6a; see Fig. 3a). This mismatch between the experiments is due to the difficulty of accurately reproducing such low concentrations of TMP in separate dilutions (TMP concentrations are tenfold lower than CMP concentrations; see Methods): low TMP in the second experiment turned out to be closer to ultralow TMP in the first experiment, and ultralow TMP in the second experiment appeared to be similar to no drug at all. This difference, however, is not essential because we nevertheless observe that some low concentration of TMP produces the same effect in both experiments.

Other comparisons of lineage dynamics between populations under the same conditions, and between different conditions, were generally similar in the experiment with constant concentrations, albeit noisier because the weaker selection pressures and shorter timescale of the second experiment produced a smaller range of lineage dynamics. For example, the rates of lineage diversity loss were once again similar across replicates under the same conditions (Extended Data Fig. 6b; see Fig. 3b), except for distortions in some comparisons (for example, low TMP replicate 2, ultralow TMP replicate 1, and no drug replicate 2) owing to noise in the lineage diversity estimates at single time points (Extended Data Fig. 6a). The smaller dynamic range of trajectories also meant that trajectory clustering was less robust (Supplementary Figs. 17 and 18), but this analysis nevertheless recovered similar patterns of pre-existing and de novo beneficial mutations (Extended Data Fig. 8).

Simulations reproduce observed lineage dynamics. To further test our interpretations of the experimental results, we simulated evolutionary dynamics of a barcoded population under a serial dilution scheme similar to the experiment (see Methods for complete details). We focused on varying the supply of pre-existing mutations, which accumulate during the preparation of the barcode library, and the supply of de novo mutations, which accumulate during the evolution experiment. In general, we found that having both types of variation was necessary to qualitatively reproduce trajectories similar to the observed experimental data (Extended Data Fig. 9; see Fig. 2 and Extended Data Fig. 4).

Although we explored a range of parameter values (mutation rates and distributions of selection coefficients of mutations) in the simulations, for simplicity we present two contrasting cases (Methods). Both cases have pre-existing as well as de novo mutations, but pre-existing mutations dominate in the first case (intended to mimic low CMP conditions), whereas de novo mutations dominate in the second case (intended to mimic no drug conditions). We simulated two replicate populations in each case. We first checked whether pre-existing and de novo mutations in the simulations led to trajectories similar to what we observed from the clustering analysis of the real data. Indeed, the simulated trajectories for these two types of lineages qualitatively match the behaviour of the observed trajectories (Supplementary Fig. 19; see Fig. 6a and Supplementary Fig. 13).

Next, we analysed the lineage diversity of the simulated populations. We calculated the effective number of lineages (equation (1)) in each of the populations over time (Extended Data Fig. 10a). As in the experiment, the simulated replicates show a high degree of reproducibility in their diversity dynamics, and the dominance of pre-existing beneficial mutations clearly accelerates the decay of diversity. This supports our interpretation of the experimental data regarding the increased role of pre-existing mutations under low CMP compared to other conditions. We also simulated populations under purely neutral dynamics and confirmed that neutral processes alone cannot reproduce the observed amount of diversity loss (see Fig. 3a). Moreover, we tested the effect of finite sampling of barcodes on the estimated diversity. That is, we subsampled 10% of each simulated population three times and calculated the lineage diversities on the basis of these subsamples (Supplementary Fig. 20). We found that the effect of subsampling was negligible, especially for $q > 0$ where lineages are weighted by their frequencies.

Finally, we calculated the lineage dissimilarity (equation (2)) across replicates in each of these conditions (Extended Data Fig. 10b). This further demonstrates how our two contrasting simulation conditions mimic the experimental data: the populations dominated by pre-existing mutations initially diverged from each other but then later converged, as seen in the low CMP population, while the populations dominated by de novo mutations simply diverged monotonically. Again, the simulated neutral populations diverged much more slowly than what we observed in the experiment (see Fig. 4b), and the effect of subsampling on the estimated dissimilarity was negligible (Supplementary Fig. 21). This analysis also supports our conclusion that the fates of individual lineages are not strongly determined by the initial frequency distribution, since the distribution used in our simulations was the same as the one measured for the real chromosomal library (Extended Data Fig. 1a). If this distribution had a dominant role in determining which lineages fixed, then we would see a high level of convergence across replicates in all cases; however, that does not happen without strongly selected pre-existing mutations.

Discussion

We have demonstrated a method that generates *E. coli* populations carrying 10^5 to 10^6 unique chromosomal barcodes. We tested the utility of the method by evolving the barcoded population in the presence of sub-inhibitory concentrations of two common antibiotics. Fitness phenotyping, especially of spontaneous single mutations, has been the major focus of previous applications of high-resolution

microbial barcoding[16]. However, this approach is applicable only under a strict set of conditions: environments must be constant, the population must start with minimal genetic diversity, and the population can be meaningfully tracked only over a short amount of time before any lineages rise to high frequency. Here we have pursued a complementary, ecology-inspired approach to high-resolution lineage tracking which focuses on measuring lineage diversity over time and between populations. Because this approach is more phenomenological, it can be applied to a wider variety of conditions, such as time-varying environments and initial populations that already contain substantial genetic diversity. Although lineage diversity has been used in some previous studies[5,19], here we have provided a comprehensive investigation of how it can be used to analyse lineage-tracking data from DNA barcodes in bacterial populations. We believe our methodology provides a valuable guide for the design and analysis of future barcoding applications in bacteria, especially for experiments involving fluctuating environments and comparisons across large numbers of environments and replicates.

We found that each drug regimen in our experiment prompted a distinct and reproducible rate of lineage diversity loss (Fig. 3), with the exception of the ultralow CMP and no drug conditions, which exhibited similar diversity loss dynamics (although they differed in other ways). Since the effect of genetic drift on the loss of lineage diversity at the population scale was limited, owing to the large size of the evolving populations ($>10^7$) and the short timescale (about 420 generations), we can interpret the rate of lineage diversity loss as a proxy for the rate of adaptation in the population. Curiously, the diversity dynamics were reproducible regardless of the rate itself; for example, both the low CMP condition, which induced the fastest rate of adaptation, and the ultralow TMP condition, which induced the slowest adaptation dynamics, exhibited high reproducibility between evolutionary replicates. This observation implies a surprisingly deterministic dynamics at the level of lineage diversity, despite differences in the distributions of fitness effects across conditions in our experiment.

One of the most surprising features of these results is that there is some range of low TMP concentrations that reduce the rate of lineage diversity loss even beyond the rate under no drug at all. While it is difficult to determine the precise concentration at which this effect occurs, owing to the low magnitude of these concentrations, we have reproduced it across replicate populations in the same experiment (Fig. 3a) as well as across populations in different evolution experiments (Extended Data Fig. 6a) to demonstrate that such conditions exist. Since the growth dynamics of these populations indicate that they experience a similar number of generations per passage as the other populations (Extended Data Fig. 2e, f), we hypothesize that the observed delay in adaptation to TMP is due to a reduction in selection coefficients on beneficial mutations, compared to both higher concentrations of TMP and to the no drug condition. A previous study estimated the distribution of selection coefficients from spontaneous mutations in *E. coli* by measuring growth rates of single-gene knockouts as a proxy[36]. This indeed also showed that the distribution of selection coefficients under TMP was narrower than the distribution under no drug. Other previous studies have suggested that, at a low dosage, antibiotics might operate not as a weapon, but rather as signalling molecules that trigger transcriptional activation of multiple genes, including genes involved in the biosynthesis of amino acids, ribosomal proteins, purines and pyrimidines[21]. If TMP, which is known to affect transcription[37], indeed induces a new metabolic state in bacterial cells at ultralow concentrations, it could potentially lead to a shift in the distribution of beneficial mutations. We expect that future work will elucidate the detailed mechanism underlying delayed adaptation in low concentrations of TMP.

An important problem in evolutionary biology is reliably quantifying the reproducibility of evolutionary processes[38,39]. Adaptation in near-lethal drug concentrations often appears to be nearly deterministic owing to the existence of a handful of strongly beneficial mutations, which repeatedly accumulate in similar orders across replicate populations[40]. However, it is more challenging to quantify the reproducibility of evolutionary dynamics when they are driven by many small-effect mutations at the whole-population level. Our chromosomal barcoding system in *E. coli* allowed us to address this problem directly by quantitatively comparing lineage dynamics across independent replicate populations subjected to identical antibiotic regimes. We found not only that the rate of lineage diversity loss was highly reproducible for each selection condition (Fig. 3), but also that the dynamics were deterministic at the level of individual lineages in some cases (Fig. 4), with a few lineages rising to high frequency in multiple independently evolving populations (Fig. 5).

Populations can adapt to new environments using two sources of variation: pre-existing mutations (that is, standing genetic variation) and de novo mutations arising after the environmental change[41]. Previous work has shown both the enrichment of pre-existing mutations[30,42] and the emergence of new resistance-conferring mutations[30,43] under sub-MIC concentrations of antibiotics. However, the relative contributions of these two sources of variation to evolutionary dynamics has remained unknown. Here we developed a quantitative approach to address this problem by measuring lineage composition dissimilarity[34,35] between replicate populations (Fig. 4) and analysis of individual lineage trajectories (Fig. 6). These results suggest that lineages present at very low frequencies in the initial population, but nonetheless independently reaching high frequency in the replicate populations, are repetitively selected because they carry pre-existing beneficial mutations. Thus, the extent of similarity in lineage composition between evolutionary replicates at a particular time point quantitatively reports on the contribution of standing genetic variation to the observed dynamics. As expected, the rapid adaptation under low CMP was accompanied by the lowest lineage dissimilarity among selection regimes (Fig. 4), indicating a substantial contribution of pre-existing mutations. Conversely, pre-existing variation has a less important role under the ultralow TMP and no drug conditions (Fig. 6c), where the evolutionary dynamics was rather driven mostly by de novo mutations.

Overall, our results demonstrate substantial evolutionary insights gleaned from high-resolution lineage tracking using chromosomal barcodes in *E. coli*. Our experimental barcoding protocol based on the Tn7 transposon machinery is straightforward to implement and can be readily be reproduced in a variety of systems. We have furthermore shown how to obtain a robust quantitative analysis of the resulting lineage data using ecological diversity indices and trajectory clustering. Altogether, we envision that this tool will find wide application in addressing diverse questions in bacterial population and evolutionary dynamics.

Methods

Design of the chromosomal barcode integration system in *E. coli*. The design of the chromosomal integration system of the barcode library is based on the pGRG25 plasmid, which carries all the components of the Tn7 transposon site-specific recombination machinery[25,44,45]. We separated the Tn7 transposase machinery (*tnsABCDE*) from the Tn7 arms (Tn7L, Tn7R) onto two independent plasmids: the temperature-sensitive 'helper' plasmid (pSC101 temperature-sensitive origin of replication) carrying the *tnsABCD* genes under the control of an arabinose-inducible pBAD promoter (Fig. 1a), and the 'integration' plasmid (R6K gamma *pir* + dependent origin of replication) with the Tn7 arms flanking the barcode-carrying cassette and spectinomycin resistance gene (Fig. 1b,c). The separation of the recombination machinery *tnsABCD* from the integration segment flanked by the Tn7 arms achieved two major goals. First, the introduction of the helper plasmid into the cells prior to the integration plasmid allowed us to precondition the cells for chromosomal recombination by inducing the expression of the transposase complex, which we expected to increase the integration efficiency. Second, the transient nature of the integration plasmid eliminated any possibility of barcodes lingering outside their designated chromosomal location owing to unsuccessfully cured plasmids (that is, plasmids no longer present in the

host cell). This is especially important for barcoding temperature-sensitive strains that cannot be grown at non-permissive temperatures.

The barcode-carrying cassette (Fig. 1c) is designed to minimize the number of library preparation steps required for Illumina deep-sequencing technology. The only variable region in the cassette is the barcode sequence of 15 random nucleotides. Thus, the barcode library has a maximum possible diversity of 4^{15} (about 10^9) unique barcodes. The barcodes are asymmetrically located 9 nucleotides downstream of the 5′ end of the cassette. This short stretch of 9 nucleotides is sufficient to locate the barcodes in the raw sequencing data files and to reduce the sequence redundancy in the Illumina flow cell. The cassette is flanked by the sequences complementary to the Illumina adapter primers used to anchor library specific indices recognized by the Illumina sequencing platforms (MiSeq, HiSeq or Nextseq) (Fig. 1c). The Integrated DNA Technology gBlocks service synthesized the barcode cassettes (allowing the incorporation of 15 consecutive and variable nucleotides), which we then cloned into the Tn7 integration plasmid (Fig. 1b). We characterized the resulting library of barcodes by deep sequencing prior to integration into the genome (Extended Data Fig. 1). We found that the actual diversity of this initial barcode library was three orders of magnitude lower than the maximal theoretical diversity (1.3×10^6 unique barcodes) (Supplementary Table 1). Although the distribution of barcode frequencies was fairly narrow (Extended Data Fig. 1a), sampling from a relatively small number of unique barcodes could have been a factor that contributed to the frequency distribution bias observed in the plasmid integration library (see below). Thus, to reduce the bias, a different approach for generating the initial barcode diversity, such as primers with diversified positions synthesized using manual mixing, can be used in the future library preparations.

Design of the barcode-carrying cassette. The barcodes consist of 15 random nucleotides each, which we placed 9 nucleotides downstream of the 5′ end of the 288-nucleotide-long cassette:

gtcgcgccggNNNNNNNNNNNNNNNtatctcggtagtgggatacgacgataccgaagacag-ctcatgttatatcccgccgttaaccaccatcaaacaggattttcgcctgctggggcaaaccagcgtggaccgcttgctgc-aactctctcagggccaggcggtgaagggcaatcagctgttgcccgtctcactggtgaaaagaaaaaccaccctggcgcc-caatacgcaaaccgcctctccccgcgcgttggccgattcattaatgcagctggcacgacaggtttccc

We placed the barcode-carrying cassette between sequences complementary to Illumina adaptor primers (forward overhang: 5′ TCGTCGGCAGCGTCAGAT GTGTATAAGAGACAG; reverse overhang: 5′ GTCTCGTGGGCTCGGAGATGT GTATAAGAGACAG) and, finally, flanked by sequences complementary to the integration site in the Tn7 integration plasmid:

gatatcggatcctagtaagccacgttttaattaatcagatccctcaatagccacaacaactggcgggcaaacag tcgttgctgattggtcgtcggcagcgtcagatgtgtataagagacagtcgcgccggNNNNNNNNNNNN NNNtatctcggtagtgggatacgacgataccgaagacagctcatgttatatcccgccgttaaccaccatcaaacag gattttcgcctgctggggcaaaccagcgtggaccgcttgctgcaactctctcagggccaggcggtgaagggcaatcagc tgttgcccgtctcactggtgaaaagaaaaaccaccctggcgcccaatacgcaaaccgcctctccccgcgcgttggcc gattcattaatgcagctggcacgacaggtttcccctgtctcttatacacatctccgagcccacgagac gccactcgagttatttgccgactaccttggtgatctcgcctttcacgtag

Integrated DNA Technology (https://www.idtdna.com/pages/products/genes-and-gene-fragments/gblocks-gene-fragments) synthesized the resulting 492-nucleotide-long sequence as double-stranded gBlocks with randomly mixed bases (at the 15 consecutive positions indicated by N).

Generation of plasmid barcode library. We digested the empty Tn7 integration plasmids with NotI, purified them by ethanol precipitation, and then mixed the plasmids with gBlocks in a 1:3 molar ratio in the presence of NEBbuilder HiFi DNA (New England Biolabs) assembly mix, according to the manufacturer's instructions. We used a control without NEBbuilder HiFi DNA assembly mix to determine the background level (Tn7 integration plasmid lacking the cassette). We concentrated the reactions by ethanol precipitation and transformed them into 100 µl of TransforMax EC100D *pir* + cells (Lucigen). We resuspended the transformed cells in 1 ml of SOC medium, regenerated them for 1 h at 37 °C with shaking followed by overnight incubation on the bench, and then plated the cells on 35 µg ml^{-1} kanamycin Luria-Bertani (LB) agar plates (100 µl of transformed cells per plate). We plated several microlitres of diluted cultures separately to determine the number of colony-forming cells. We incubated plates overnight at 37 °C. Cells transformed with DNA but without the assembly mix produced no colonies. Transformation of DNA with the assembly mix generated a total of about 2.4×10^6 colonies (Fig. 1d). We scraped all the colonies from the plates, pooled them together and thoroughly mixed them. Finally, we extracted plasmids from the pooled cells with a Qiagen midi kit.

Chromosomal integration of the barcode library into *E. coli* cells. This is a two-step process, the first step being the transformation of the recipient *E. coli* MG1655 cells with the Tn7 helper plasmid and induction of the transposase integration machinery. The second step is the transformation of the Tn7 integration plasmid library, which integrates the barcodes into the chromosome (Fig. 1d). We grew cells transformed with the Tn7 helper plasmid overnight until saturation in LB supplemented with 100 µg ml^{-1} ampicillin at 30 °C. We then diluted these cells 1:100 and grew them under the same conditions for 45 min. We added 0.2% arabinose and diluted cells to an optical density at 600 nm of 0.5. We then harvested the cells, washed them three times with ice-cold water and transformed them with the Tn7 integration plasmid library using electroporation. We resuspended the transformed cells in 1 ml of SOC medium, regenerated them for 1 h at 30 °C with shaking followed by overnight incubation on the bench, and then plated them on 100 µg ml^{-1} spectinomycin LB agar plates (100 µl of transformed cells per plate). We plated several microlitres of diluted culture separately to determine the number of colony-forming cells. We incubated plates overnight at 37 °C and produced ~2×10^6 colonies in total. All randomly picked colonies (over 50) failed to grow on ampicillin, suggesting that overnight incubation at 37 °C is sufficient to cure the majority of cells of the Tn7 helper plasmids. Similarly, we observed no growth on kanamycin, showing that the Tn7 integration plasmids were no longer present. We further validated the chromosomal incorporation of the barcode-carrying cassettes by colony PCR with a pair of primers directed to the Tn7 integration site. All randomly picked colonies (over 50) were positive for the chromosomal integration. We scraped all the colonies from the plates, pooled them together, thoroughly mixed them, aliquoted them with 15% glycerol and stored them at −80 °C.

As shown in Extended Data Fig. 1a, chromosomal incorporation of the plasmid library reduced the number of unique barcodes and increased the barcode frequency bias. We believe that the major source of this perturbation is the extensive variation in the size of individual colonies on agar plates, which translates into differences of orders of magnitude in the number of individual cells. Indeed, each individual grown colony can consist of 10^6 to 10^9 individual cells[46]. In principle, we can substantially reduce such variation by shortening the incubation time of the chromosomal library on the agar plates from 16 h to only 6–7 h. This approach produces micro-colonies with much smaller variation in the colony sizes, as was previously demonstrated[47].

Deep sequencing of the gBlocks library, the Tn7 integration plasmid library and the naive barcoded *E. coli* population. Sample preparation for deep sequencing involved four steps. First, we amplified the barcode-carrying cassettes with Illumina adaptor primers (forward adaptor: 5′ TCGTCGGCAGCGTCAGA TGTGTATAAGAGACAG; reverse adaptor: 5′ GTCTCGTGGGCTCGGAGAT GTGTATAAGAGACAG). We used gBlocks and the Tn7 integration plasmid library directly as DNA templates in the PCR reaction. In the case of the naive barcoded *E. coli* population, we performed the PCR reaction either directly on the cells or, alternatively, on the genomic DNA extracted from the barcoded population with Nucleospin Microbial DNA prep kit (Machary-Nagel), using the manufacturer's instructions. The PCR reaction mix was prepared as follows: combine 1 µl (250 U) PrimeSTAR GXL DNA polymerase (TaKaRa), 1 µl 10 ng µl^{-1} Adaptor_forward primer, 1 µl 10 ng µl^{-1} Adaptor_reverse primer, 10 µl 5× reaction buffer, 4 µl 2.5 mM dNTPs, 50 ng genomic DNA or 3 µl bacterial culture, and bring to 50 µl with water. The PCR amplification conditions were: one cycle of 94 °C for 5 min, then 30 cycles each of 95 °C for 10 s, 55 °C for 15 s and 68 °C for 45 s, followed by one cycle of 68 °C for 5 min.

In the second step, we separated the PCR products on 1% agarose gel, then excised and purified it with a NucleoSpin Gel extraction kit (Machary-Nagel) following the manufacturer's instructions. Third, we subjected the gel-purified product of the first PCR reaction to a second PCR reaction using a unique air of index primers (i5 and i7) from Nextera XT DNA library preparation kit (Illumina), as follows: 1 µl (250 U) PrimeSTAR GXL DNA polymerase (TaKaRa), 5 µl Nextera XT index1 i7 primer, 5 µl Nextera XT index2 i5 primer, 10 µl 5× reaction buffer, 4 µl 2.5 mM dNTPs, 55 ng DNA and bring to 50 µl with water. The PCR amplification conditions were: one cycle of 94 °C for 5 min, then 12 cycles each of 95 °C for 10 s, 55 °C for 15 s and 68 °C for 45 s, followed by one cycle of 68 °C for 5 min.

In the fourth and final step, we purified the product of the second PCR reaction with Agencourt AMPure XP PCR purification kit (Beckman Coulter). We performed sequencing on MiSeq or NextSeq platforms (Illumina).

Laboratory evolution. We subjected the naive barcoded *E. coli* population to laboratory evolution via serial passaging under five distinct growth conditions: low CMP (1–3 µg ml^{-1}), ultralow CMP (0.1 µg ml^{-1}), low TMP (0.1–1.2 µg ml^{-1}), ultralow TMP (0.01–0.1 µg ml^{-1}), and no drug (Extended Data Fig. 2a,b). We gradually increased the concentrations of the antibiotics throughout the evolution experiment to sustain a relatively constant level of cell density for the low CMP and low TMP conditions. To this end, upon completion of each growth cycle, we measured the cell density of the evolving populations by optical density (OD) at 600 nm. Once the cell density of the populations grown under the low CMP and low TMP conditions increased beyond ~80% of that of the populations under the no drug condition, we increased the concentration of the corresponding antibiotic by ~30%–50% (Supplementary Fig. 3).

We grew cells at 37 °C in a 96-well microtitre plate (500 µl per well) in supplemented M9 medium (0.2% glucose, 1 mM $MgSO_4$, 0.1% casamino acids, 0.5 mg ml^{-1} thiamin). Between passages, we grew cultures for 8–9 h (during the day) or 10–12 h (during the night). We used saturated culture from a previous passage to inoculate a fresh plate by 1:100 dilution (5 µl of saturated culture into 500 µl of fresh medium). Under these conditions, cultures reached saturation within ~6 h of growth. Thus, during the alternating growth cycles of 8–9 h and 10–12 h, cultures spent at a stationary phase in the incubator under the growth conditions between

2–3 h and 4–6 h, respectively. Overall, we performed 70 passages. We measured the optical density of the cultures at 600 nm at the end of each passage (Supplementary Table 2). We convert the raw optical density measurements to an estimated number of cells (Extended Data Fig. 2c,d) as follows: we first multiply by 10 to correct for dilution of the measured culture, then multiply by 2 to standardize the optical density to the 1-cm path length, then multiply by cell density (that is, 10^8 cells per ml per unit of optical density), and finally multiply by 0.2 ml (that is, the volume of the well). We stored every second passage at −80 °C after addition of 15% glycerol.

We also repeated the evolution experiment with all drug concentrations held constant: low CMP at 1 μg ml^{-1}, ultralow CMP at 0.1 μg ml^{-1}, low TMP at 0.1 μg ml^{-1}, ultralow TMP at 0.01 μg ml^{-1} as well a condition with no drug. As before we propagated 14 identical cultures per condition. We grew cells at 37 °C in a 96-well microtitre plate (500 μl per well) in supplemented M9 medium (0.2% glucose, 1 mM $MgSO_4$, 0.1% casamino acids, 0.5 mg ml^{-1} thiamin). For these experiments, we performed serial passaging of the cultures consistently every 12 h. To this end, we used the saturated culture from a previous passage to inoculate a fresh plate by 1:100 dilution (5 μl of saturated culture into 500 μl of fresh medium). Overall, we performed 30 passages and stored every second passage at −80 °C after addition of 15% glycerol.

Growth measurements of the evolving barcoded *E. coli* populations. We estimated resistance of the evolving populations by calculating the change in IC50 of CMP or TMP, following the methodology in ref. [48]. We sampled cells from three populations each under the low CMP, ultralow CMP and no drug conditions at passages 0, 8, 10, 12, 20, 30 and 70. We diluted these samples 1:100 into growth medium supplemented with 0 μg ml^{-1}, 1 μg ml^{-1}, 2 μg ml^{-1}, 4 μg ml^{-1}, 8 μg ml^{-1} or 16 μg ml^{-1} of CMP, and followed their growth by optical density measurements at 600 nm (Supplementary Fig. 4a, Supplementary Table 3). We calculated the area under these growth curves over the time of growth (Supplementary Fig. 4b) and normalized the area values so that they equalled 1 at zero antibiotic (Supplementary Fig. 4c). We determined the IC50 by calculating the concentration of antibiotic at which growth (defined as normalized area under the growth curve) was reduced by 50% relative to zero antibiotic (Supplementary Fig. 4c). We inferred the IC50 concentration by interpolating the area versus drug concentration curves. We similarly obtained IC50 values for three populations each for the low TMP, ultralow TMP and no drug conditions at the same time points, but with TMP concentrations 0 μg ml^{-1}, 0.5 μg ml^{-1}, 1 μg ml^{-1}, 2 μg ml^{-1}, 5 μg ml^{-1}, 10 μg ml^{-1} and 20 μg ml^{-1} (Supplementary Table 3).

Deep sequencing of the evolving barcoded *E. coli* populations. We sequenced barcodes at 16 time points over the evolution experiment for the same 15 independent populations used for the growth measurements. We first amplified these 240 bacterial cultures with Illumina adaptor primers (15 μl of defrosted cells from each culture). We performed the second PCR in two groups, each with 96 unique Nextera XT primers. We then pooled together 96 PCR reactions from each group, spiked them with 30% of PhiX DNA, and sequenced them on a Nextseq High Output 75 platform. The sequencing protocol commenced with nine dark cycles to account for the sequence redundancy preceding the barcode area. For one sample (ultralow CMP, replicate 2, passage 54) all PCR reactions failed, and thus we excluded this sample from all further analysis.

Analysis of sequencing data. First, we exclude sequencing samples that report fewer than 10^6 reads; this affects six time points from the evolving populations (Supplementary Table 1). All remaining samples have between 1.3×10^6 and 1.4×10^7 reads. Next, we exclude all reads with minimum base quality score less than 10 (Phred scale), which affects 0.02%–0.16% of reads (Supplementary Table 1). To identify barcodes, we first align each read to the reference sequence for the barcode cassette. We allow up to three mismatches or one indel with respect to the reference; we also require that the read overlap the barcode by at least 10 nucleotides. With these criteria we identify barcodes on more than 95% of reads in all but 17 samples from the original experiment (Supplementary Table 1). For each read with a valid alignment, we extract a barcode as the sequence aligning to the variable region in the reference.

To correct for sequencing errors in the raw barcodes, we use the bartender package[49] on default settings to cluster together barcodes with similar sequences. In general, this method assumes that a low-frequency barcode differing at only one or two bases from a high-frequency barcode is the result of a sequencing error, so that the low-frequency barcode is merged into the high-frequency one. This produces a set of putative true barcodes for the sample.

To ensure that we identify true barcodes consistently across samples, we first pool raw barcodes and perform clustering on these pooled samples. We pool barcodes both across time points for each population (to build trajectories of barcodes over time in each population) as well as across populations for each time point (to compare barcodes between populations). After clustering, we disaggregate the true barcodes from the pooled data back into the individual samples, where we normalize them by the total number of reads in that sample. This yields a set of lineage frequencies $\{x_k(t)\}$ (where the index k runs over all barcodes) for each population at each time point t.

Quantifying lineage diversity. The simplest way to quantify the diversity of barcoded lineages in a population is to count the number of unique barcodes observed at a particular time point (Fig. 3a). However, if lineages differ widely in frequency, then this measure may not be very informative and will suffer from substantial sampling bias (since very low-frequency barcodes will be under-sampled). A more general approach is to define the effective number of lineages using the diversity index ${}^qD$ from ecology[34]. We construct this definition in analogy with the case where all lineages are at equal frequency, so that the number of lineages is simply the reciprocal of this frequency:

$$\text{number of lineages} = \frac{1}{\text{frequency of each lineage}} \tag{3}$$

When lineages are not at equal frequencies, we replace the frequency in the denominator by a mean frequency over all lineages. Define the generalized mean (also known as the power mean) of a quantity h_k, with normalized weights p_k $\left(\sum_k p_k = 1\right)$ and parameter q:

$$\langle h_k|p_k,q\rangle = \left(\sum_k p_k h_k^{q-1}\right)^{1/(q-1)} \tag{4}$$

The parameter q controls how strongly the mean depends on very small or very large values of h_k: lower values of q allow relatively more weight from low values of h_k, while higher values of q more strongly weight high values of h_k. When $q=2$, equation (4) reduces to the ordinary arithmetic mean; when $q=1$, it is equivalent to the geometric mean; and when $q=0$, it is the harmonic mean.

We therefore define the effective number of lineages as the reciprocal of the generalized mean frequency over all lineages, weighting each frequency by itself[34,35]:

$${}^qD = \frac{1}{\langle x_k|x_k,q\rangle} = \left(\sum_{\text{lineage }k} x_k^q\right)^{1/(1-q)} \tag{5}$$

The diversity index is mathematically equivalent to the exponential of the Renyi entropy in physics[50]. Special values of the parameter q correspond to common ecological measures of diversity:

$$q=0: \quad {}^qD = \text{number of lineages with nonzero frequency (species richness)} \tag{6}$$

$$q=1: \quad {}^qD = \exp\left(-\sum\nolimits_{\text{lineage }k} x_k \log x_k\right) \text{(Shannon diversity)} \tag{7}$$

$$q=2: \quad {}^qD = \left(\sum\nolimits_{\text{lineage }k} x_k^2\right)^{-1} \text{(reciprocal mean frequency, also known as Simpson concentration)} \tag{8}$$

$$q=\infty: \quad {}^qD = \frac{1}{\max_{\text{lineage }k} x_k} \tag{9}$$

We note that the effective number of lineages according to equation (5) equals the actual number of lineages for any q if all lineages have equal frequency. Figure 3 shows the diversity indices for $q=0$, $q=1$ and $q=\infty$ for each population over the course of the evolution experiment.

Quantifying dissimilarity of lineage composition between populations. We can also use diversity indices to quantitatively compare the lineage compositions of two or more populations. Let M be the number of populations we are comparing ($M\geq2$), and let $x_k^{(p)}$ be the frequency of lineage k in population $p=(1,2,\ldots,M)$ at a particular time point. If we pool together all M populations, the frequency of lineage k is:

$$\bar{x}_k = \frac{1}{M}\sum_{\text{population }p} x_k^{(p)} \tag{10}$$

The total diversity of the pooled population (gamma diversity) is[34,35]:

$${}^qD_{\text{pooled}} = \frac{1}{\langle \bar{x}_k|\bar{x}_k,q\rangle} = \left(\sum_k \bar{x}_k^q\right)^{1/(1-q)} \tag{11}$$

We can decompose this total diversity into two factors:

$${}^qD_{\text{pooled}} = {}^qD_{\text{mean}}\,{}^qM_{\text{eff}} \tag{12}$$

The first factor on the right-hand side of equation (12) is the mean diversity across all populations (alpha diversity):

$$ {}^{q}D_{\mathrm{mean}} = \frac{1}{\left\langle \frac{1}{{}^{q}D^{(p)}} \right\rangle^{\frac{1}{M},q}} = \left(\frac{1}{M} \sum_{\text{population } p} \left[{}^{q}D^{(p)} \right]^{1-q} \right)^{\frac{1}{1-q}} \quad (13) $$

where ${}^{q}D^{(p)}$ is the diversity of population p alone (equation (5)). The second factor on the right-hand side of equation (12) is the effective number of distinct populations (beta diversity):

$$ {}^{q}M_{\mathrm{eff}} = \frac{{}^{q}D_{\mathrm{pooled}}}{{}^{q}D_{\mathrm{mean}}} = \left(\frac{\sum_{\text{lineage } k} \bar{x}_k^q}{\frac{1}{M}\sum_{\text{population } p} \sum_{\text{lineage } k} \left[x_k^{(p)} \right]^q} \right)^{1/(1-q)} \quad (14) $$

This quantity has a minimum value of 1 if the populations have identical lineages at identical frequencies, and a maximum value of M if none of the populations have any lineages in common. To simplify the interpretation of this quantity across cases where we may be comparing different numbers of populations, we shift and rescale ${}^{q}M_{\mathrm{eff}}$ to obtain a measure of dissimilarity between populations that ranges from 0 to 1:

$$ \frac{{}^{q}M_{\mathrm{eff}} - 1}{M - 1} \quad (15) $$

We plot this normalized quantity in all figures (Fig. 4, Extended Data Fig. 7, Extended Data Fig. 10 and Supplementary Figs. 5, 6, 10 and 21).

In the case of $q = 0$, ${}^{0}M_{\mathrm{eff}}$ simply measures how many lineages with nonzero frequency are in common between the populations under comparison. Let $B^{(p)}$ be the set of lineages with nonzero frequencies in population p, and let $|B^{(p)}|$ denote the number of lineages in this set. Then the effective number of distinct populations is:

$$ {}^{0}M_{\mathrm{eff}} = \frac{\left| \cup_{\text{population } p} B^{(p)} \right|}{\frac{1}{M}\sum_{\text{population } p} |B^{(p)}|} \quad (16) $$

For two populations ($M = 2$), we can rewrite this as:

$$ {}^{0}M_{\mathrm{eff}} = \frac{\left| B^{(1)} \cup B^{(2)} \right|}{\frac{1}{2}\left(|B^{(1)}| + |B^{(2)}| \right)} = 2 - \frac{1}{\frac{1}{2}\left(\frac{|B^{(1)}|}{|B^{(1)} \cap B^{(2)}|} + \frac{|B^{(2)}|}{|B^{(1)} \cap B^{(2)}|} \right)} \quad (17) $$

where we have invoked the inclusion-exclusion principle for sets $|B^{(1)} \cup B^{(2)}| = |B^{(1)}| + |B^{(2)}| - |B^{(1)} \cap B^{(2)}|$. That is, ${}^{0}M_{\mathrm{eff}}$ equals two minus the harmonic mean of the fractions of overlapping lineages between the populations. For example, ${}^{q}M_{\mathrm{eff}} = 1.8$ means that the two populations have 20% of their lineages in common.

In the case of $q = 1$, the effective number of lineages is the Shannon diversity (equation (7)). Therefore the effective number of distinct populations is equivalent to the exponential of the Jensen–Shannon divergence between the populations:

$$ {}^{1}M_{\mathrm{eff}} = \exp\left[\frac{1}{M} \sum_{\text{population } p} \sum_{\text{lineage } k} x_k^{(p)} \log\left(\frac{x_k^{(p)}}{\bar{x}_k} \right) \right] \quad (18) $$

This is also equivalent to the weighted sum of the Kullback–Leibler divergences between each population and the pooled population.

In the case of $q = \infty$, the effective number of distinct populations depends only on the most abundant lineage in the pooled population and across all populations. That is,

$$ {}^{\infty}D_{\mathrm{pooled}} = \frac{1}{\max_{\text{lineage } k} \bar{x}_k} \quad (19) $$

and

$$ {}^{\infty}D_{\mathrm{mean}} = \frac{1}{\max_{\text{population } p} \max_{\text{lineage } k} x_k^{(p)}} \quad (20) $$

and so

$$ {}^{\infty}M_{\mathrm{eff}} = \frac{\max_{\text{population } p} \max_{\text{lineage } k} x_k^{(p)}}{\max_{\text{lineage } k} \bar{x}_k} \quad (21) $$

Clustering lineage frequency trajectories. For each population from the original experiment, we exclude barcoded lineages that have zero detected frequency at more time points than a minimum number calculated as:

$$ \lfloor 0.5(\text{total number of time points} + 11) \rfloor \quad (22) $$

where $\lfloor\ \rfloor$ is the floor function that rounds the argument down to the nearest integer. This ensures that all pairs of remaining lineages have at least ten time points at which they both have nonzero frequency. This leaves between 177 and 969 lineages for each population. For the evolution experiment with constant drug conditions, we take the top 500 lineages ranked by mean frequency over time. In both cases we cluster the frequency trajectories $\{x_k(t)\}$ for these lineages using the hierarchical clustering routine in SciPy[51]. The distance metric between two lineages k_1 and k_2 is:

$$ \Delta(x_{k_1}(t), x_{k_2}(t)) = 1 - \rho(\log x_{k_1}(t), \log x_{k_2}(t))) \quad (23) $$

where $\rho(\log x_{k_1}(t), \log x_{k_2}(t)))$ is the Pearson correlation coefficient between the logarithms of both frequency trajectories (excluding time points where either frequency is zero); Supplementary Fig. 11 shows matrices of all pairwise trajectory correlations, while Supplementary Fig. 12 shows this data in histogram form. Supplementary Fig. 17 shows the same data but for the evolution experiment with constant drug conditions. We use the 'average' linkage method (equivalent to the unweighted pair group method with arithmetic mean, or UPGMA), which calculates the distance between two clusters as the arithmetic mean of the distances between all trajectories in both clusters. Other linkage methods produce qualitatively similar results. The hierarchical clustering results in dendrograms as shown in Supplementary Figs. 11 and 17. Finally, we form flat clusters by setting thresholds on the dendrograms, which we manually choose for each population; these thresholds are shown on the dendrograms in Supplementary Fig. 11 and range from 0.15 to 0.65, which roughly means that the minimum correlations between trajectories within clusters ranges from 0.35 to 0.85. For the evolution experiment with constant drug conditions, we set these thresholds to be 0.06 (minimum correlation 0.94) for all populations (Supplementary Fig. 17), since the smaller dynamic range of the trajectories creates a greater risk of over-clustering.

Simulations. We performed all simulations with SodaPop[52] using a multiplicative fitness function. We first accounted for the evolutionary dynamics during the barcode library preparation. We evolved 10^7 cells, all initially clonal, for 30 generations, which corresponds to the approximate number of generations accrued during preparation of the barcode library on the *E. coli* chromosomes (Fig. 1d). We set the rate of arising mutations to $\mu = 10^{-5}$ per genome per generation, reflecting estimates of beneficial mutation rates in bacteria[53,54]. We assumed that mutations arising during this period were neutral during library preparation but contained a cryptic selection coefficient effect s that is only realized during evolution under drug conditions. We randomly drew these cryptic selection coefficients from an exponential distribution. At the end of the simulated library preparation, we randomized the cell indices and sequentially assigned barcodes to the cells, using the experimentally measured distribution of chromosomal barcode frequencies (Extended Data Fig. 1a). From these initial populations, we then simulated the evolution experiment itself for 400 generations.

While we tested a range of parameter values for these simulations, here we focus on just two cases that qualitatively reproduce the range of phenomena we observe in the experiments, along with a control condition of purely neutral population dynamics. We call the first case 'pre-existing dominated', since the evolutionary dynamics are primarily driven by beneficial mutations already present at the beginning of the evolution experiment, rather than de novo mutations acquired during the experiment. In this case, we use $s = 0.05$ as the mean selection coefficient for pre-existing mutations arising during library preparation. De novo mutations occur during the evolution experiment at rate $\mu = 2.5 \times 10^{-4}$ and are chosen to be deleterious with probability 0.9 and beneficial with probability 0.1; for either type of mutation, we draw the selection coefficient from an exponential distribution with mean $s = \pm 0.05$. The second case is 'de novo dominated', since de novo mutations during the evolution experiment mainly drive the dynamics. In this case, we use $s = 0.01$ as the mean selection coefficient for pre-existing mutations, while de novo mutations occur at the rate $\mu = 10^{-5}$ and are strictly beneficial with an exponential distribution of mean $s = 0.01$. For both of these conditions as well as the neutral control case, we simulated two replicate populations.

Reporting Summary. Further information on research design is available in the Nature Research Reporting Summary linked to this article.

Data availability

All raw barcode sequencing data used in this study is deposited in the National Center for Biotechnology Information Sequence Read Archive under BioProject accession numbers PRJNA592527 (initial barcode libraries), PRJNA592371 (time points from evolution experiment under increasing drug concentrations), and PRJNA592529 (time points from evolution experiment under constant drug concentrations). All other raw data is included in Supplementary Tables 1–4.

Code availability

All custom scripts used to analyse the data are available on request.

Received: 5 March 2019; Accepted: 8 January 2020;
Published online: 24 February 2020

References

1. Lazar, V. et al. Genome-wide analysis captures the determinants of the antibiotic cross-resistance interaction network. *Nat Commun.* **5**, 4352 (2014).
2. Deatherage, D. E. & Barrick, J. E. Identification of mutations in laboratory-evolved microbes from next-generation sequencing data using breseq. *Methods Mol. Biol.* **1151**, 165–188 (2014).
3. Otto, M. Next-generation sequencing to monitor the spread of antimicrobial resistance. *Genome Med.* **9**, 68 (2017).
4. Xue, Y. & Wilcox, W. R. Changing paradigm of cancer therapy: precision medicine by next-generation sequencing. *Cancer Biol. Med.* **13**, 12–18 (2016).
5. Blundell, J. R. et al. The dynamics of adaptive genetic diversity during the early stages of clonal evolution. *Nat. Ecol. Evol.* **3**, 293–301 (2018).
6. Desai, M. M., Walczak, A. M. & Fisher, D. S. Genetic diversity and the structure of genealogies in rapidly adapting populations. *Genetics* **193**, 565–585 (2013).
7. Lang, G. I., Botstein, D. & Desai, M. M. Genetic variation and the fate of beneficial mutations in asexual populations. *Genetics* **188**, 647–661 (2011).
8. Neher, R. A. & Hallatschek, O. Genealogies of rapidly adapting populations. *Proc. Natl Acad. Sci. USA* **110**, 437–442 (2013).
9. Fox, E. J., Reid-Bayliss, K. S., Emond, M. J. & Loeb, L. A. Accuracy of next generation sequencing platforms. *Next Gener. Seq. Appl.* **1**, 1000106 (2014).
10. Pfeiffer, F. et al. Systematic evaluation of error rates and causes in short samples in next-generation sequencing. *Sci. Rep.* **8**, 10950 (2018).
11. Hegreness, M., Shoresh, N., Hartl, D. & Kishony, R. An equivalence principle for the incorporation of favorable mutations in asexual populations. *Science* **311**, 1615–1617 (2006).
12. Stannek, L., Egelkamp, R., Gunka, K. & Commichau, F. M. Monitoring intraspecies competition in a bacterial cell population by cocultivation of fluorescently labelled strains. *J. Vis. Exp.* **83**, e51196 (2014).
13. Wetmore, K. M. et al. Rapid quantification of mutant fitness in diverse bacteria by sequencing randomly bar-coded transposons. *MBio* **6**, e00306–e00315 (2015).
14. Blundell, J. R. & Levy, S. F. Beyond genome sequencing: lineage tracking with barcodes to study the dynamics of evolution, infection, and cancer. *Genomics* **104**, 417–430 (2014).
15. Jaffe, M., Sherlock, G. & Levy, S. F. iSeq: a new double-barcode method for detecting dynamic genetic interactions in yeast. *G3* **7**, 143–153 (2017).
16. Levy, S. F. et al. Quantitative evolutionary dynamics using high-resolution lineage tracking. *Nature* **519**, 181–186 (2015).
17. Peikon, I. D., Gizatullina, D. I. & Zador, A. M. In vivo generation of DNA sequence diversity for cellular barcoding. *Nucleic Acids Res.* **42**, e127 (2014).
18. Jahn, L. J. et al. Chromosomal barcoding as a tool for multiplexed phenotypic characterization of laboratory evolved lineages. *Sci. Rep.* **8**, 6961 (2018).
19. Cira, N. J., Pearce, M. T. & Quake, S. R. Neutral and selective dynamics in a synthetic microbial community. *Proc. Natl Acad. Sci. USA* **115**, E9842–E9848 (2018).
20. Andersson, D. I. & Hughes, D. Microbiological effects of sublethal levels of antibiotics. *Nat. Rev. Microbiol.* **12**, 465–478 (2014).
21. Davies, J., Spiegelman, G. B. & Yim, G. The world of subinhibitory antibiotic concentrations. *Curr. Opin. Microbiol.* **9**, 445–453 (2006).
22. Fajardo, A. & Martinez, J. L. Antibiotics as signals that trigger specific bacterial responses. *Curr. Opin. Microbiol.* **11**, 161–167 (2008).
23. Thomason, L. C., Sawitzke, J. A., Li, X., Costantino, N. & Court, D. L. Recombineering: genetic engineering in bacteria using homologous recombination. *Curr. Protoc. Mol. Biol.* **106**, 11–39 (2014).
24. Choi, K. H. & Schweizer, H. P. mini-Tn7 insertion in bacteria with single *attTn7* sites: example *Pseudomonas aeruginosa*. *Nat. Protoc.* **1**, 153–161 (2006).
25. McKenzie, G. J. & Craig, N. L. Fast, easy and efficient: site-specific insertion of transgenes into enterobacterial chromosomes using Tn7 without need for selection of the insertion event. *BMC Microbiol.* **6**, 39 (2006).
26. Baquero, F., Alvarez-Ortega, C. & Martinez, J. L. Ecology and evolution of antibiotic resistance. *Environ. Microbiol. Rep.* **1**, 469–476 (2009).
27. Baquero, F. & Negri, M. C. Selective compartments for resistant microorganisms in antibiotic gradients. *Bioessays* **19**, 731–736 (1997).
28. Wolfe, A. D. & Hahn, F. E. Mode of action of chloramphenicol. IX. Effects of chloramphenicol upon a ribosomal amino acid polymerization system and its binding to bacterial ribosome. *Biochim. Biophys. Acta* **95**, 146–155 (1965).
29. Brogden, R. N., Carmine, A. A., Heel, R. C., Speight, T. M. & Avery, G. S. Trimethoprim: a review of its antibacterial activity, pharmacokinetics and therapeutic use in urinary tract infections. *Drugs* **23**, 405–430 (1982).
30. Gullberg, E. et al. Selection of resistant bacteria at very low antibiotic concentrations. *PLoS Pathog.* **7**, e1002158 (2011).
31. Andersson, D. I. & Hughes, D. Evolution of antibiotic resistance at non-lethal drug concentrations. *Drug Resist. Upd.* **15**, 162–172 (2012).
32. Bjorkman, J. & Andersson, D. I. The cost of antibiotic resistance from a bacterial perspective. *Drug Resist. Upd.* **3**, 237–245 (2000).
33. Crow, J. F. & Kimura, M. *An Introduction To Population Genetics Theory* (Harper & Row, 1970).
34. Jost, L. Entropy and diversity. *Oikos* **113**, 363–375 (2006).
35. Tuomisto, H. A diversity of beta diversities: straightening up a concept gone awry. Part 1. Defining beta diversity as a function of alpha and gamma diversity. *Ecography* **33**, 2–22 (2010).
36. Chevereau, G. et al. Quantifying the determinants of evolutionary dynamics leading to drug resistance. *PLoS Biol.* **13**, e1002299 (2015).
37. Bershtein, S., Choi, J. M., Bhattacharyya, S., Budnik, B. & Shakhnovich, E. Systems-level response to point mutations in a core metabolic enzyme modulates genotype-phenotype relationship. *Cell Rep.* **11**, 645–656 (2015).
38. de Visser, J. A. & Krug, J. Empirical fitness landscapes and the predictability of evolution. *Nat. Rev. Genet.* **15**, 480–490 (2014).
39. Lobkovsky, A. E. & Koonin, E. V. Replaying the tape of life: quantification of the predictability of evolution. *Front. Genet.* **3**, 246 (2012).
40. Toprak, E. et al. Evolutionary paths to antibiotic resistance under dynamically sustained drug selection. *Nat. Genet.* **44**, 101–105 (2011).
41. Barrett, R. D. & Schluter, D. Adaptation from standing genetic variation. *Trends Ecol. Evol.* **23**, 38–44 (2008).
42. Liu, A. et al. Selective advantage of resistant strains at trace levels of antibiotics: a simple and ultrasensitive color test for detection of antibiotics and genotoxic agents. *Antimicrob. Agents Chemother.* **55**, 1204–1210 (2011).
43. Westhoff, S. et al. The evolution of no-cost resistance at sub-MIC concentrations of streptomycin in *Streptomyces coelicolor*. *ISME J* **11**, 1168–1178 (2017).
44. McKown, R. L., Orle, K. A., Chen, T. & Craig, N. L. Sequence requirements of *Escherichia coli attTn7*, a specific site of transposon Tn7 insertion. *J. Bacteriol.* **170**, 352–358 (1988).
45. Peters, J. E. & Craig, N. L. Tn7: smarter than we thought. *Nat. Rev. Mol. Cell Biol.* **2**, 806–814 (2001).
46. Mashimo, K., Nagata, Y., Kawata, M., Iwasaki, H. & Yamamoto, K. Role of the RuvAB protein in avoiding spontaneous formation of deletion mutations in the *Escherichia coli* K-12 endogenous *tonB* gene. *Biochem. Biophys. Res. Commun.* **323**, 197–203 (2004).
47. Bershtein, S., Segal, M., Bekerman, R., Tokuriki, N. & Tawfik, D. S. Robustness-epistasis link shapes the fitness landscape of a randomly drifting protein. *Nature* **444**, 929–932 (2006).
48. Palmer, A. C. et al. Delayed commitment to evolutionary fate in antibiotic resistance fitness landscapes. *Nat. Commun.* **6**, 7385 (2015).
49. Zhao, L., Liu, Z., Levy, S. F. & Wu, S. Bartender: a fast and accurate clustering algorithm to count barcode reads. *Bioinformatics* **34**, 739–747 (2018).
50. Rényi, A. On measures of information and entropy. *Proc. Fourth Berkeley Symp. Mathematics, Statistics and Probability* 547–561 (Univ. California Press, 1960).
51. Virtanen, P. et al. SciPy 1.0--Fundamental algorithms for scientific computing in Python. Preprint at https://arxiv.org/abs/1907.10121 (2019).
52. Gauthier, L., Di Franco, R. & Serohijos, A. W. R. SodaPop: a forward simulation suite for the evolutionary dynamics of asexual populations on protein fitness landscapes. *Bioinformatics* **35**, 4053–4062 (2019).
53. Fogle, C. A., Nagle, J. L. & Desai, M. M. Clonal interference, multiple mutations and adaptation in large asexual populations. *Genetics* **180**, 2163–2173 (2008).
54. Perfeito, L., Fernandes, L., Mota, C. & Gordo, I. Adaptive mutations in bacteria: high rate and small effects. *Science* **317**, 813–815 (2007).
55. Gibson, D. G. et al. Enzymatic assembly of DNA molecules up to several hundred kilobases. *Nat. Methods* **6**, 343–345 (2009).
56. Gibson, D. G. et al. Creation of a bacterial cell controlled by a chemically synthesized genome. *Science* **329**, 52–56 (2010).
57. Datsenko, K. A. & Wanner, B. L. One-step inactivation of chromosomal genes in *Escherichia coli* K-12 using PCR products. *Proc. Natl Acad. Sci. USA* **97**, 6640–6645 (2000).

Acknowledgements

We thank L. Zhao, J. Rojas Echenique, S. Levy and A. Pascual Garcia for advice on analysing the data, and D. Tawfik and A. Aharoni for comments and help with preparation of the manuscript. This work was supported by an F32 fellowship from the US National Institutes of Health (GM116217) and an Ambizione grant from the Swiss National Science Foundation (PZ00P3_180147) to M.M.; a grant from the Canadian Natural Sciences and Engineering Research Council (NSERC RN000524) to A.W.R.S.; and a personal Israel Science Foundation grant 1630/15 to S.B. We also acknowledge support from the FAS Division of Science, Research Computing Group at Harvard University for the computations performed on the Odyssey cluster.

Author contributions

S.B. conceived the study. W.J. and J.L. performed the laboratory experiments. M.M. analysed sequencing data and developed ecological approach. L.G. and A.W.R.S.

performed simulations. M.M., L.G., A.W.R.S. and S.B. interpreted the data. M.M. and S.B. wrote the manuscript. All authors approved of the final manuscript.

Competing interests
The authors declare no competing interests.

Additional information
Extended data is available for this paper at https://doi.org/10.1038/s41559-020-1103-z.

Supplementary information is available for this paper at https://doi.org/10.1038/s41559-020-1103-z.

Correspondence and requests for materials should be addressed to S.B.

Reprints and permissions information is available at www.nature.com/reprints.

Publisher's note Springer Nature remains neutral with regard to jurisdictional claims in published maps and institutional affiliations.

© The Author(s), under exclusive licence to Springer Nature Limited 2020

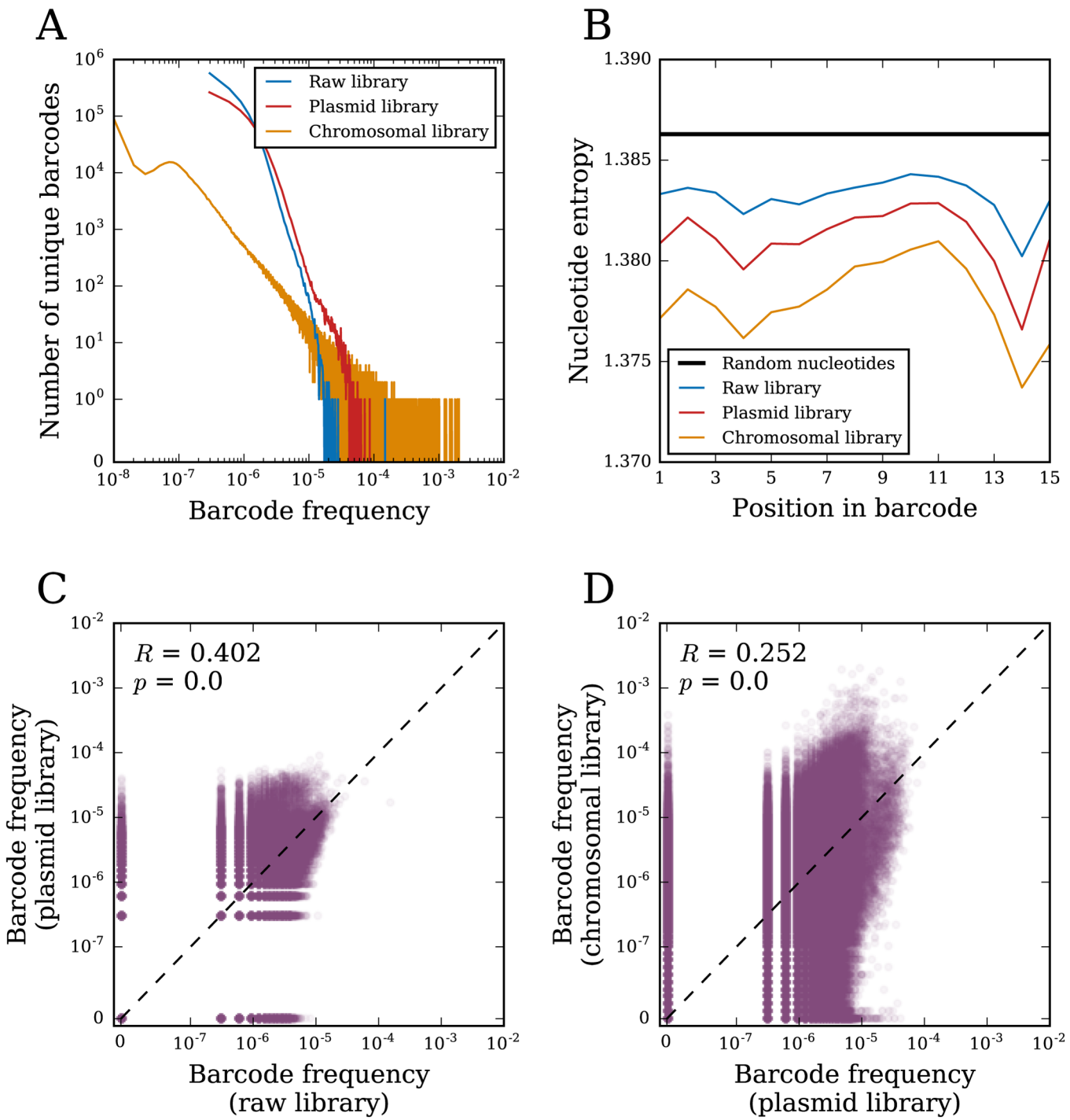

Extended Data Fig. 1 | Initial barcode libraries. (A) Distributions of barcode frequencies at different stages of library preparation. For a given frequency on the horizontal axis, the vertical axis shows the number of unique detected barcodes with that frequency. "Raw library" (blue): NextSeq Illumina sequencing of the barcode library as synthesized by IDT (prior to plasmid library creation). "Plasmid library" (red): MiSeq Illumina sequencing of barcodes incorporated into the Tn7 integration plasmid library. "Chromosomal library" (orange): NextSeq Illumina sequencing of the barcode library integrated into *E. coli* chromosomes and generated by PCR performed on chromosomal DNA pooled from four independent extractions. **(B)** Shannon entropy of nucleotides at each position in the 15 nt barcode for the same libraries in panel (A). The horizontal black line marks the entropy (ln 4≈1.386) of a maximally-random library where all nucleotides are equally abundant at each position. **(C)** Comparison of individual barcode frequencies in the raw library and in the plasmid library. Points are partially transparent to show their density; the dashed black line marks the line of identity. We also show the Pearson correlation coefficient *R* and estimated *p*-value for the frequencies (*p*-values are numerically indistinguishable from zero). **(D)** Same as (C) but comparing the plasmid library and the chromosomal library.

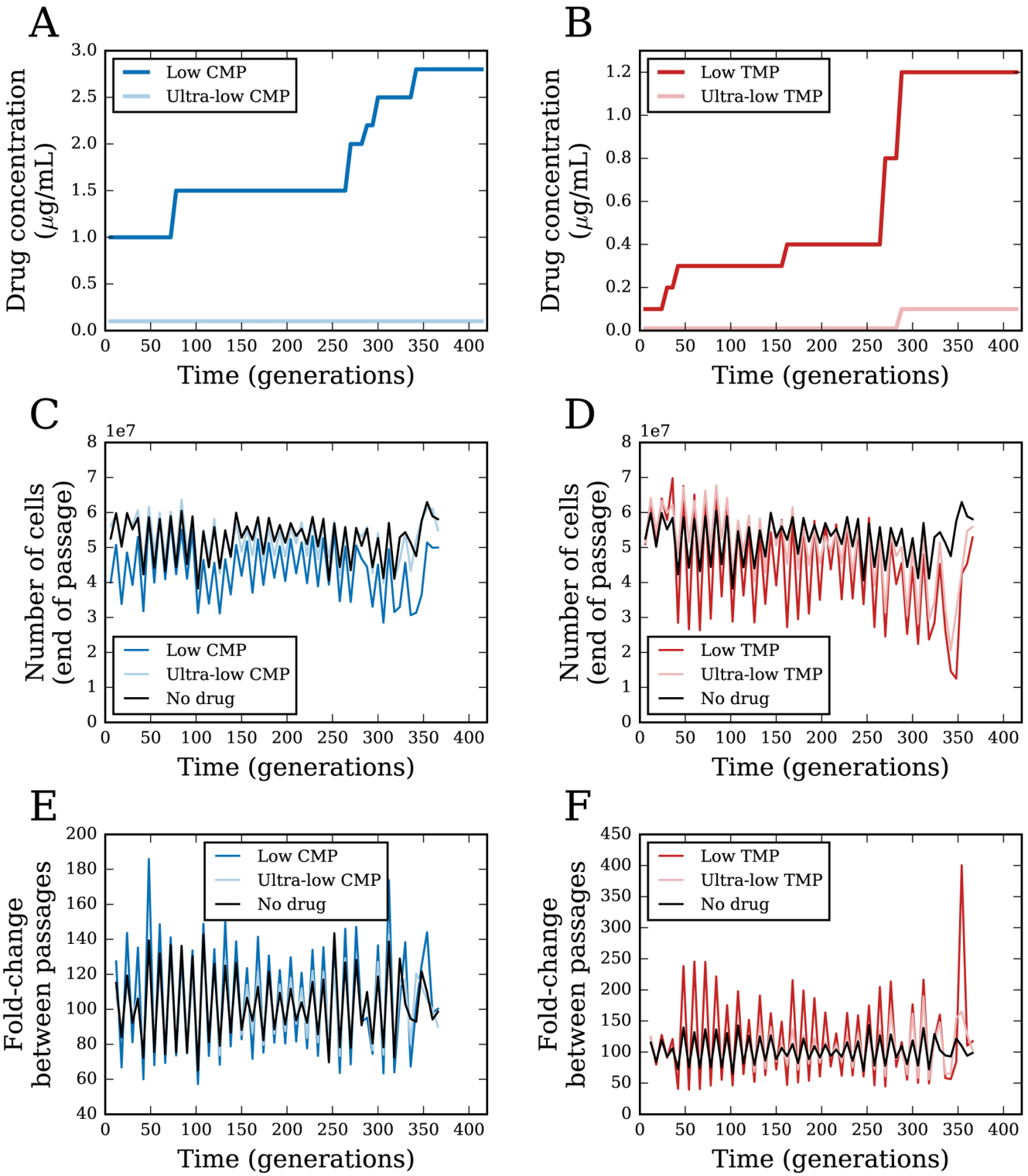

Extended Data Fig. 2 | Drug concentrations and population growth over evolution experiment. (A) Trajectories of low and ultra-low chloramphenicol (CMP) concentrations over time of the evolution experiment. **(B)** Same as (A) but for trimethoprim (TMP) conditions. **(C)** Approximate number of cells at the end of each passage for low and ultra-low CMP conditions, along with the populations evolved without drug. Lines are averages over all 14 replicate populations for each condition. **(D)** Same as (C) but for TMP conditions. **(E)** Same as (C) but showing the fold-change of population size during each passage on the vertical axis. **(F)** Same as (E) but for TMP conditions. Periodic oscillations in cell numbers and yields result from the fact that cultures were propagated in two intermittent growth regimes: 9 hours during the day, followed by 12 hours during the night (see Methods). Supplementary Table 2 contains raw OD data for each population at the end of each passage.

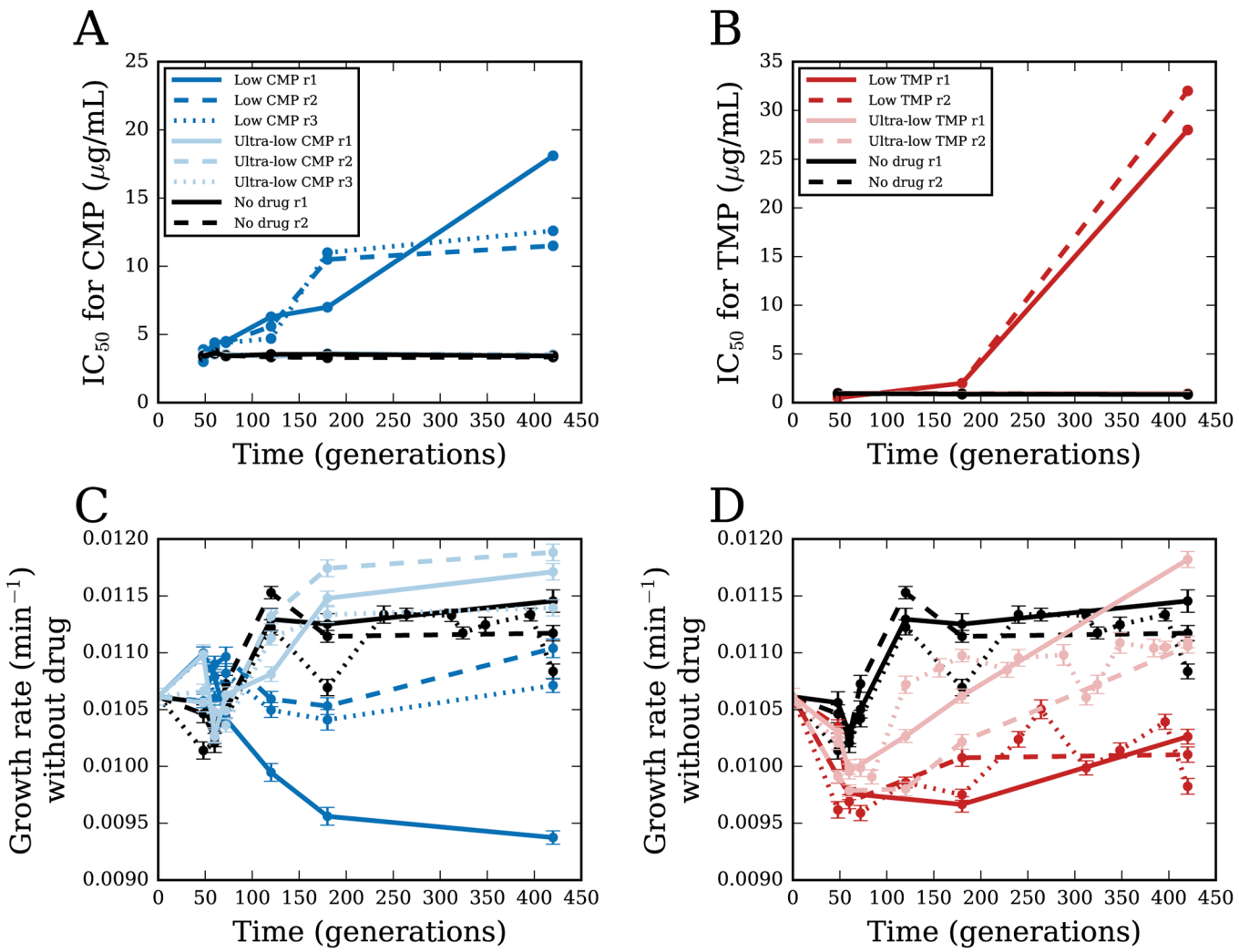

Extended Data Fig. 3 | Evolution of resistance and growth traits. (A) At several time points during the evolution experiment, we measured the chloramphenicol (CMP) IC50 of the barcoded populations evolved in low and ultra-low CMP as well as those evolving without drug. **(B)** Same as (A) but for trimethoprim (TMP). **(C)** Growth rate, measured in the absence of drug, of barcoded populations evolved in low and ultra-low CMP as well as without drug. Points represent the mean and error bars represent standard deviation over replicate measurements. **(D)** Same as (C) but for populations evolved in low and ultra-low TMP. Supplementary Table 3 contains raw growth curve data for the evolved populations at these different drug concentrations.

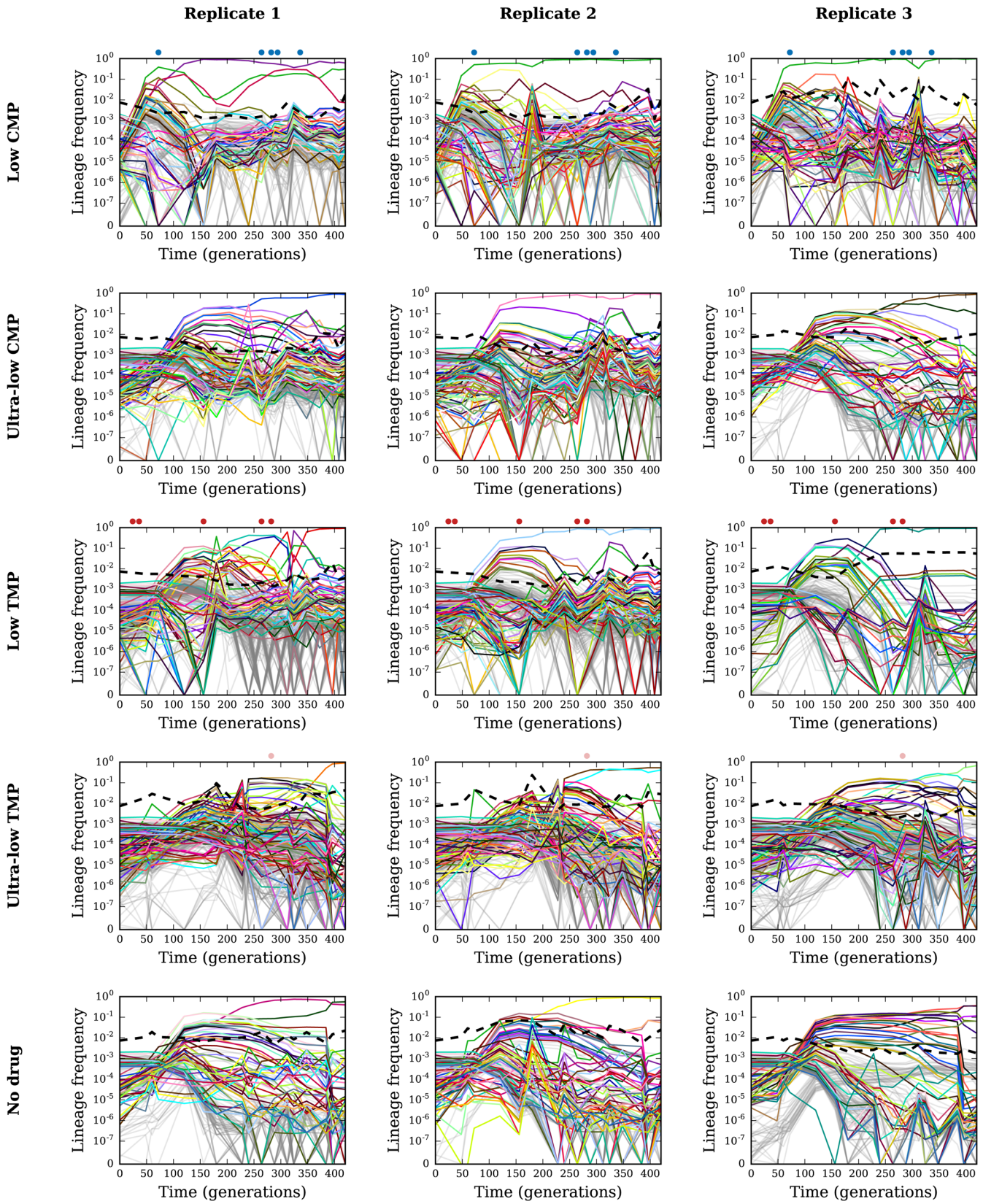

Extended Data Fig. 4 | Trajectories of barcoded lineage frequencies. Each row corresponds to a different antibiotic regimen, while each column corresponds to a different replicate. Individual panels show the frequency trajectories for barcoded lineages in single populations over time of the experiment; we only show lineages with mean frequency over time greater than 10^{-4}. For the top 20 lineages in each population (ranked by mean frequency over time), we assign a unique color to each lineage that is consistent across panels, i.e., the same color represents the same barcode across panels (Supplementary Table 4). All lower-frequency lineages are gray and partially transparent to show their density. The dashed black line represents the frequency of reads without identified barcodes. Dots above each plot mark times at which the drug concentration for that population changed (Extended Data Fig. 2A,B).

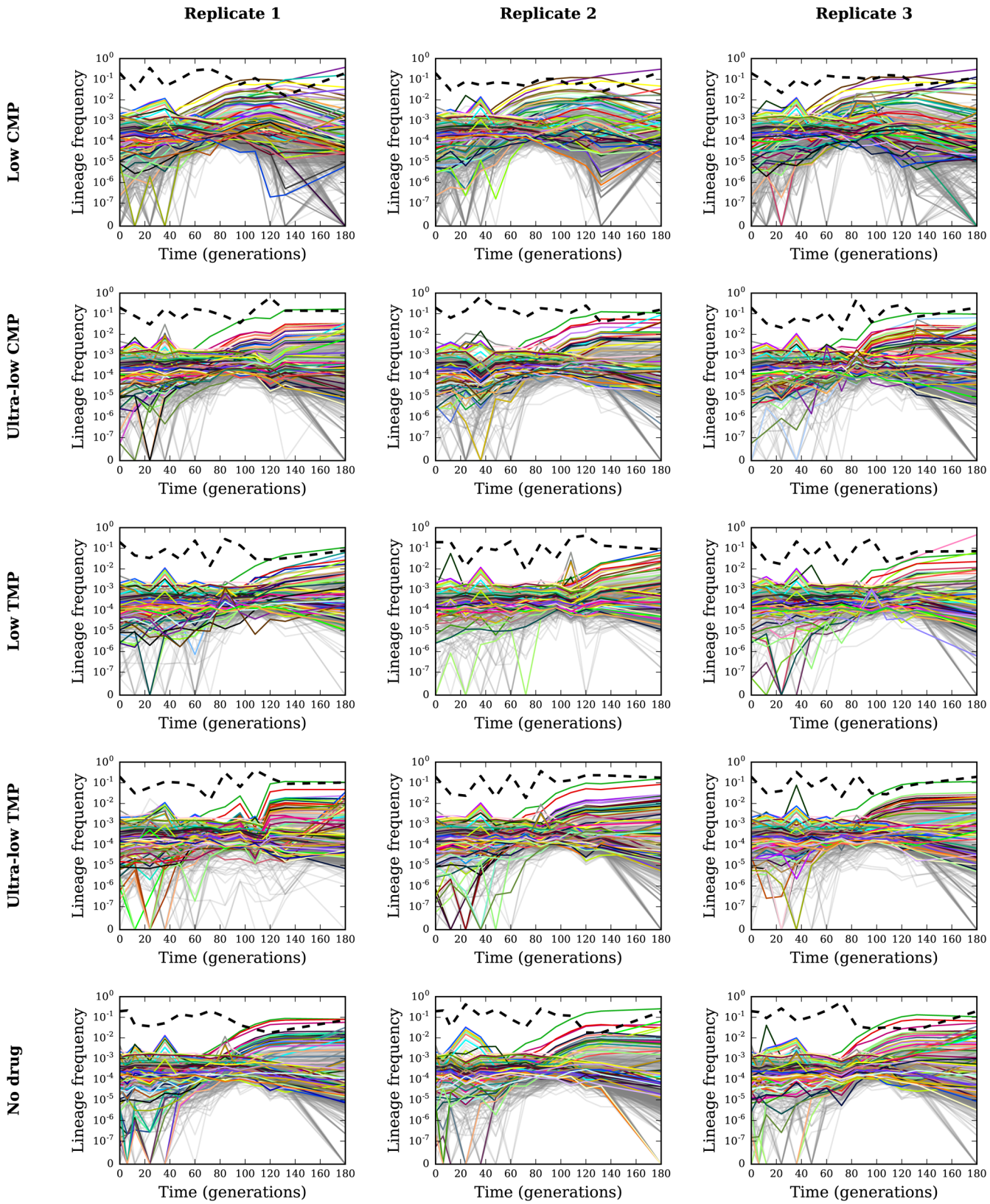

Extended Data Fig. 5 | Trajectories of barcoded lineage frequencies under constant conditions. Same as Extended Data 4 but for evolution experiments with constant drug concentrations (see Methods).

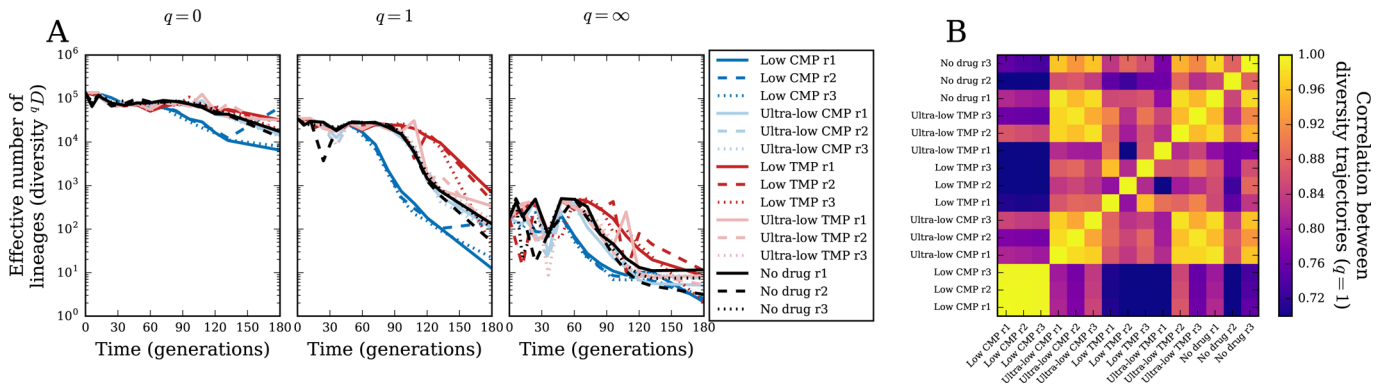

Extended Data Fig. 6 | Dynamics of lineage diversity over time under constant conditions. Same as Fig. 3 but for evolution experiments with constant drug concentrations (see Methods).

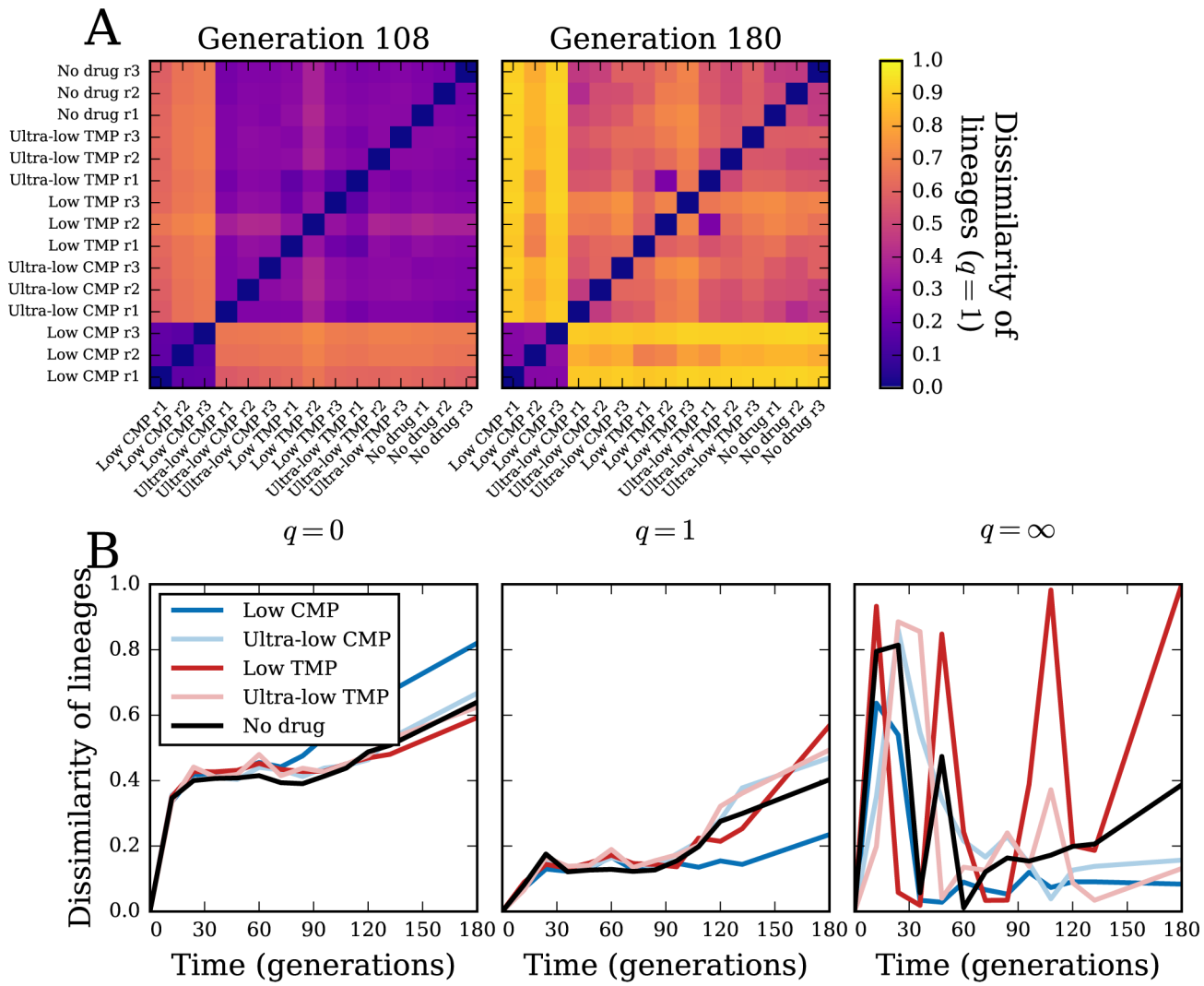

Extended Data Fig. 7 | Dynamics of lineage dissimilarity among populations over time under constant conditions. Same as Fig. 4 but for evolution experiments with constant drug concentrations (see Methods).

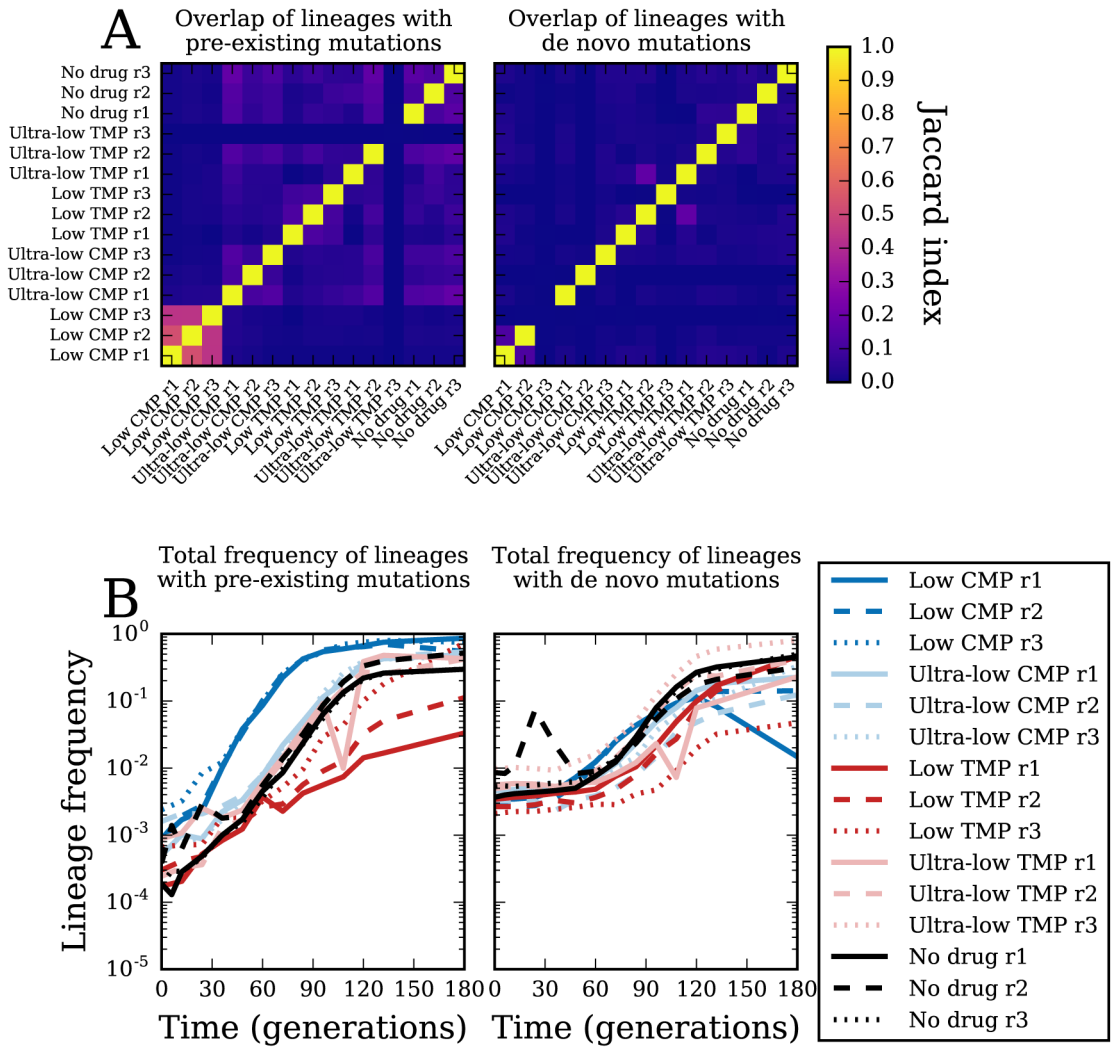

Extended Data Fig. 8 | Trajectories with pre-existing and de novo beneficial mutations under constant conditions. Same as Fig. 6B,C but for evolution experiments with constant drug concentrations (see Methods).

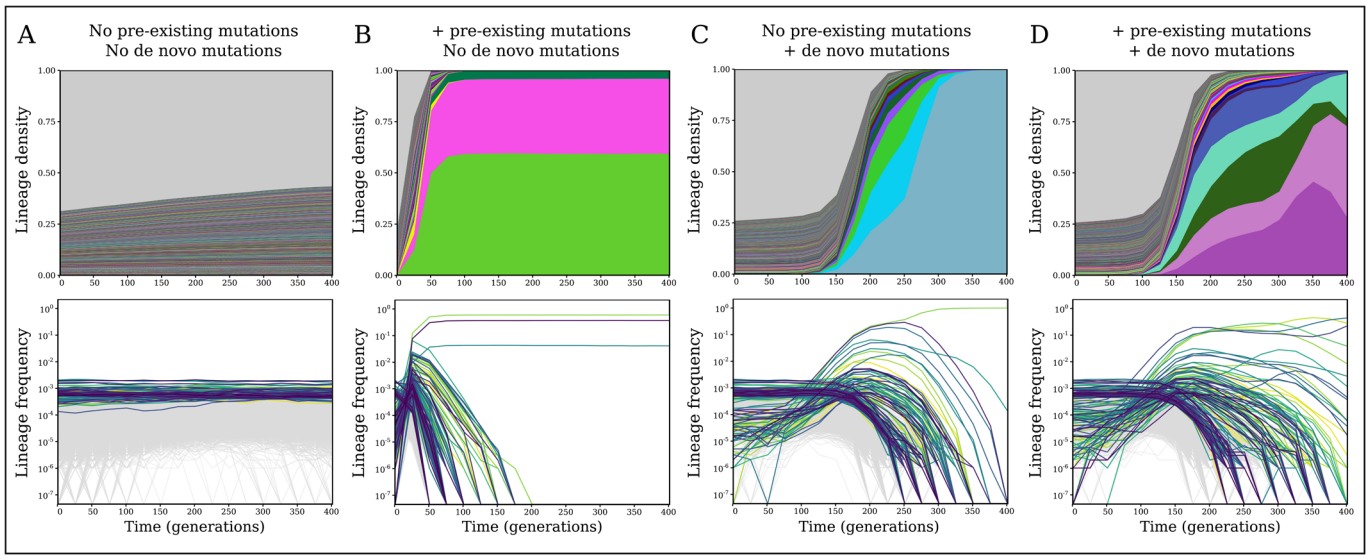

Extended Data Fig. 9 | Comparison of simulations with different sources of variation. We simulated evolutionary dynamics of a barcoded population (see Methods) with different supplies of mutations. We plot trajectories of barcoded lineage frequencies over time for simulated populations with **(A)** neither pre-existing nor de novo mutations (neutral dynamics), **(B)** pre-existing mutations only (mean s=0.1), **(C)** de novo mutations only (mean s=0.05), and **(D)** both pre-existing mutations (mean s=0.01) and de novo mutations (mixed exponential distribution with 90% deleterious and 10% beneficial). In the top row, each color indicates the relative frequency of a particular lineage at every time point. For simplicity, we show only lineages with a minimum frequency of 10^{-4} (the gray area covers the frequency of all remaining lineages). In the bottom row, we show the frequency trajectories as lines on a log scale; lineages with a minimum frequency of 5×10^{-4} are colored while all other lineages above 10^{-4} are gray. Lineage frequencies represent the estimated frequency from subsampling 10% of the full simulated population.

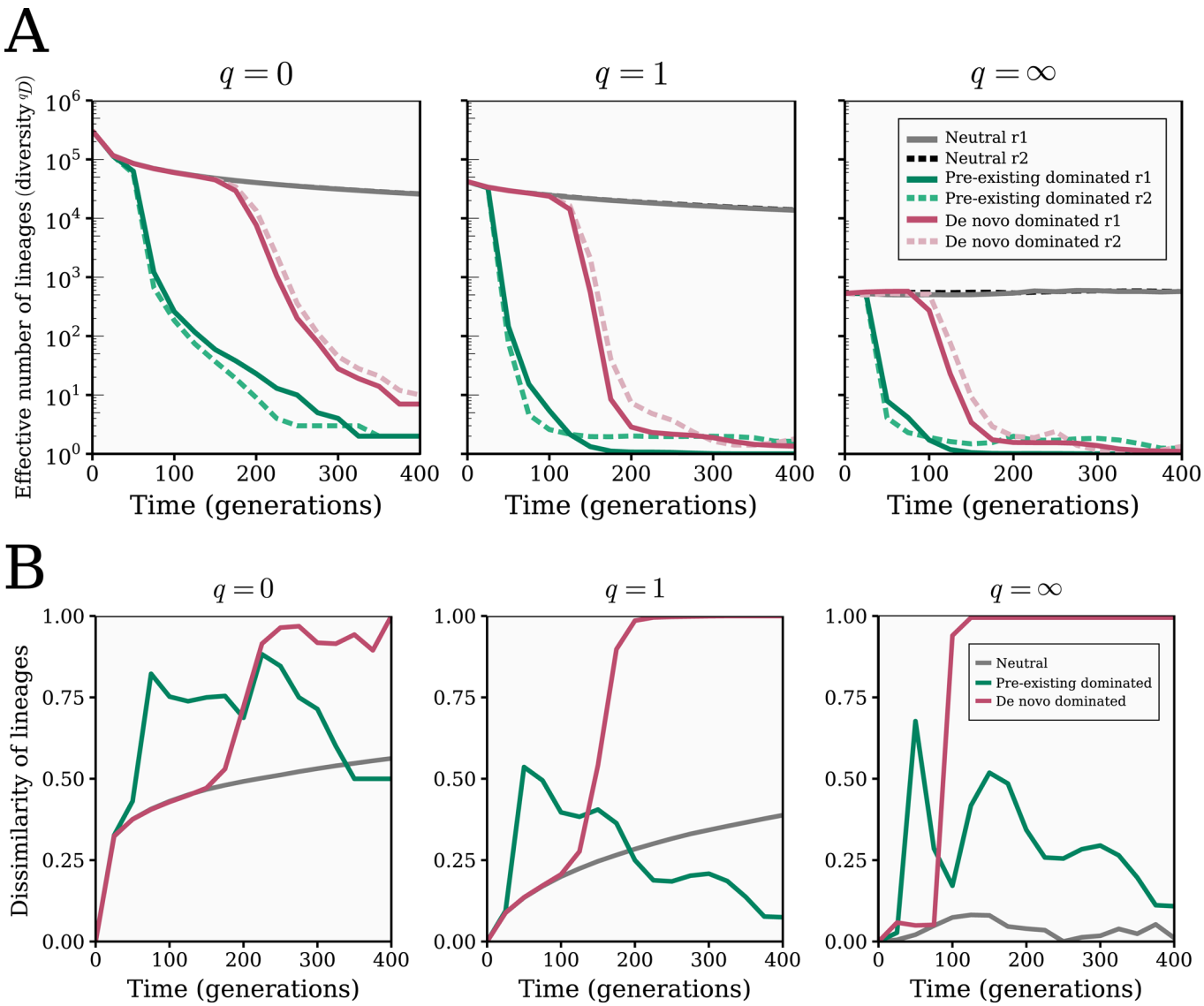

Extended Data Fig. 10 | Simulated dynamics of lineage diversity. We simulated evolutionary dynamics of the barcoded population for two replicates of each condition: "neutral" (no mutations), "pre-existing dominated," and "de novo dominated" (see Methods). **(A)** For each population, we calculated the effective number of barcoded lineages using the diversity index ^qD (Eq. 1; see also Methods) for three different values of q, which controls the weight of low- versus high-frequency lineages: ^0D (number of unique barcodes, left), ^1D (Shannon diversity, center), and $^\infty D$ (reciprocal of the maximum lineage frequency, right). **(B)** We also calculated the dissimilarity of lineages (Eq. 2; see also Methods) among all replicate populations in each condition, using q=0 (left), q=1 (center), and q=∞ (right). All diversity and dissimilarity values are based on perfect sampling of the population.

nature research

Corresponding author(s): Shimon Bershtein

Last updated by author(s): Nov 29, 2019

Reporting Summary

Nature Research wishes to improve the reproducibility of the work that we publish. This form provides structure for consistency and transparency in reporting. For further information on Nature Research policies, see Authors & Referees and the Editorial Policy Checklist.

Statistics

For all statistical analyses, confirm that the following items are present in the figure legend, table legend, main text, or Methods section.

n/a	Confirmed
☐	☒ The exact sample size (*n*) for each experimental group/condition, given as a discrete number and unit of measurement
☐	☒ A statement on whether measurements were taken from distinct samples or whether the same sample was measured repeatedly
☐	☒ The statistical test(s) used AND whether they are one- or two-sided *Only common tests should be described solely by name; describe more complex techniques in the Methods section.*
☒	☐ A description of all covariates tested
☐	☒ A description of any assumptions or corrections, such as tests of normality and adjustment for multiple comparisons
☐	☒ A full description of the statistical parameters including central tendency (e.g. means) or other basic estimates (e.g. regression coefficient) AND variation (e.g. standard deviation) or associated estimates of uncertainty (e.g. confidence intervals)
☐	☒ For null hypothesis testing, the test statistic (e.g. *F*, *t*, *r*) with confidence intervals, effect sizes, degrees of freedom and *P* value noted *Give P values as exact values whenever suitable.*
☒	☐ For Bayesian analysis, information on the choice of priors and Markov chain Monte Carlo settings
☒	☐ For hierarchical and complex designs, identification of the appropriate level for tests and full reporting of outcomes
☒	☐ Estimates of effect sizes (e.g. Cohen's *d*, Pearson's *r*), indicating how they were calculated

Our web collection on statistics for biologists contains articles on many of the points above.

Software and code

Policy information about availability of computer code

Data collection	We did not use any software to collect data.
Data analysis	For clustering barcode sequences, we used bartender version 1.1, which is freely-available on GitHub and cited in the paper. For all other analysis, we used custom code written in Python, relying on SciPy version 0.18.0 (including for hierarchical clustering and statistical tests) and NumPy version 1.11.1. All details in these scripts that are important to the analysis (e.g., mathematical equations) are documented in the paper.

For manuscripts utilizing custom algorithms or software that are central to the research but not yet described in published literature, software must be made available to editors/reviewers. We strongly encourage code deposition in a community repository (e.g. GitHub). See the Nature Research guidelines for submitting code & software for further information.

Data

Policy information about availability of data

All manuscripts must include a data availability statement. This statement should provide the following information, where applicable:

- Accession codes, unique identifiers, or web links for publicly available datasets
- A list of figures that have associated raw data
- A description of any restrictions on data availability

All raw barcode sequencing data used in this study is deposited in the National Center for Biotechnology Information Sequence Read Archive under BioProject accession numbers PRJNA592527 (initial barcode libraries), PRJNA592371 (time points from evolution experiment under increasing drug concentrations), and PRJNA592529 (time points from evolution experiment under constant drug concentrations). All other raw data is included in Supplementary Tables 1-4. All custom scripts used to analyze the data are available on request.

Field-specific reporting

Please select the one below that is the best fit for your research. If you are not sure, read the appropriate sections before making your selection.

☐ Life sciences ☐ Behavioural & social sciences ☒ Ecological, evolutionary & environmental sciences

For a reference copy of the document with all sections, see nature.com/documents/nr-reporting-summary-flat.pdf

Ecological, evolutionary & environmental sciences study design

All studies must disclose on these points even when the disclosure is negative.

Study description	We inserted barcode sequences into the chromosomes of E. coli cells and sequenced them over time to track lineages during adaptation to various antibiotic regimens.
Research sample	We used a standard laboratory strain of E. coli K-12 MG1655 since our study is primarily proof of a concept.
Sampling strategy	We evolved the largest possible number of replicates (14) for each condition given technical constraints of the evolution experiments. We then randomly chose 3 of these replicates in each condition for sequencing. These numbers of replicates were dictated by the costs of sequencing, but were justified a posteriori by their reproducibility.
Data collection	Weronika Jasinska and Jesse Lerner collected all data. Sequencing was performed at the University of Montreal and Weizmann Institute.
Timing and spatial scale	We performed the evolution experiments starting on December 16, 2016 and ending on January 24, 2017. The populations were diluted and resuspended in fresh media twice a day, once in the morning and once in the evening.
Data exclusions	We excluded time points from the sequencing data that produced fewer than 1e6 reads. This cutoff was determined a posteriori because it separated a small number of sequencing samples from the rest of the data. We have checked that inclusion or exclusion of these time points has no meaningful effect on our results, since our conclusions are largely drawn from the trends over time, which are robust to noise at individual time points.
Reproducibility	We evolved 14 replicates in each condition, and sequenced 3 of these. Our manuscript describes in detail the extent to which these replicates show similar behavior. We also performed replicate sequencing runs on the same sample to determine the reproducibility of our barcode identification. Overall we found that it is highly reproducible at the sequencing depth we use.
Randomization	Not applicable
Blinding	Not applicable

Did the study involve field work? ☐ Yes ☒ No

Reporting for specific materials, systems and methods

We require information from authors about some types of materials, experimental systems and methods used in many studies. Here, indicate whether each material, system or method listed is relevant to your study. If you are not sure if a list item applies to your research, read the appropriate section before selecting a response.

Materials & experimental systems

n/a	Involved in the study
☒	☐ Antibodies
☒	☐ Eukaryotic cell lines
☒	☐ Palaeontology
☒	☐ Animals and other organisms
☒	☐ Human research participants
☒	☐ Clinical data

Methods

n/a	Involved in the study
☒	☐ ChIP-seq
☒	☐ Flow cytometry
☒	☐ MRI-based neuroimaging